Plant Communications
Research article

CellPress
Partner Journal

FtsH4 protease controls biogenesis of the PSII complex by dual regulation of high light-inducible proteins

Vendula Krynická[1,*], Petra Skotnicová[1], Philip J. Jackson[2,3], Samuel Barnett[2], Jianfeng Yu[4], Anna Wysocka[1,5], Radek Kaňa[1], Mark J. Dickman[3], Peter J. Nixon[4], C. Neil Hunter[2] and Josef Komenda[1]

[1]The Czech Academy of Sciences, Institute of Microbiology, Centre Algatech, Novohradská 237, 379 01 Třeboň, Czech Republic

[2]Plants, Photosynthesis and Soil, School of Biosciences, University of Sheffield, Sheffield S10 2TN, UK

[3]Department of Chemical and Biological Engineering, University of Sheffield, Sheffield S1 3JD, UK

[4]Sir Ernst Chain Building-Wolfson Laboratories, Department of Life Sciences, South Kensington Campus, Imperial College London, London SW7 2AZ, UK

[5]Faculty of Science, University of South Bohemia, 370 05 České Budějovice, Czech Republic

***Correspondence: Vendula Krynická (krynicka@alga.cz)**

https://doi.org/10.1016/j.xplc.2022.100502

ABSTRACT

FtsH proteases are membrane-embedded proteolytic complexes important for protein quality control and regulation of various physiological processes in bacteria, mitochondria, and chloroplasts. Like most cyanobacteria, the model species *Synechocystis* sp. PCC 6803 contains four FtsH homologs, FtsH1–FtsH4. FtsH1–FtsH3 form two hetero-oligomeric complexes, FtsH1/3 and FtsH2/3, which play a pivotal role in acclimation to nutrient deficiency and photosystem II quality control, respectively. FtsH4 differs from the other three homologs by the formation of a homo-oligomeric complex, and together with *Arabidopsis thaliana* AtFtsH7/9 orthologs, it has been assigned to another phylogenetic group of unknown function. Our results exclude the possibility that *Synechocystis* FtsH4 structurally or functionally substitutes for the missing or non-functional FtsH2 subunit in the FtsH2/3 complex. Instead, we demonstrate that FtsH4 is involved in the biogenesis of photosystem II by dual regulation of high light-inducible proteins (Hlips). FtsH4 positively regulates expression of Hlips shortly after high light exposure but is also responsible for Hlip removal under conditions when their elevated levels are no longer needed. We provide experimental support for Hlips as proteolytic substrates of FtsH4. Fluorescent labeling of FtsH4 enabled us to assess its localization using advanced microscopic techniques. Results show that FtsH4 complexes are concentrated in well-defined membrane regions at the inner and outer periphery of the thylakoid system. Based on the identification of proteins that co-purified with the tagged FtsH4, we speculate that FtsH4 concentrates in special compartments in which the biogenesis of photosynthetic complexes takes place.

Key words: thylakoid, photosystem II biogenesis, FtsH4, high light-inducible protein, proteolysis

Krynická V., Skotnicová P., Jackson P.J., Barnett S., Yu J., Wysocka A., Kaňa R., Dickman M.J., Nixon P.J., Hunter C.N., and Komenda J. (2023). FtsH4 protease controls biogenesis of the PSII complex by dual regulation of high light-inducible proteins. Plant Comm. **4**, 100502.

INTRODUCTION

FtsHs are transmembrane metalloproteases universally conserved in bacteria, chloroplasts, and mitochondria. FtsHs have an essential function in protein turnover and processing and are involved in many biological processes that contribute to the maintenance of cellular homeostasis. In many bacteria, they are crucial for cell viability (1). In all photosynthetic organisms, they play an important role in maintaining functional photosynthesis, especially through quality control of the photosystem II (PSII) complex (Yi et al., 2022). In plants, they were also shown to participate in photosystem I (PSI) biogenesis (Jarvi et al., 2016) and in an early stage of plastid development (Kato et al., 2007). However, most of the mechanisms by which FtsHs control these

Published by the Plant Communications Shanghai Editorial Office in association with Cell Press, an imprint of Elsevier Inc., on behalf of CSPB and CEMPS, CAS.

cellular processes remain to be clarified. Like other cyanobacteria, the model species *Synechocystis* sp. PCC 6803 (hereafter *Synechocystis*) contains four FtsH homologs, FtsH1–FtsH4. Phylogenetic analysis of the FtsH sequences of various prokaryotic and eukaryotic organisms revealed three potentially orthologous groups (Shao et al., 2018). Three out of four cyanobacterial FtsHs (FtsH1–FtsH3) were assigned to an early diverging group 1, which contains FtsHs found exclusively in cyanobacteria and photosynthetic eukaryotes, including *Arabidopsis thaliana* orthologs FtsH2/8 and FtsH1/5. FtsHs from group 1 are known to participate in PSII repair (Komenda et al., 2012; Nishimura et al., 2016). In contrast to all other FtsH homologs, FtsH4 has been assigned to group 2, along with *A. thaliana* FtsH orthologs AtFtsH7/9, which are localized in the chloroplast envelope membrane (Ferro et al., 2010), and other non-photosynthetic, mostly eukaryotic FtsH sequences. The function of FtsH group 2 in photosynthetic organisms remains unclear.

Our previous research focused on the FtsH1–FtsH3 homologs, which, *in vivo*, form two hetero-oligomeric complexes, FtsH1/3 and FtsH2/3 (Boehm et al., 2012). The FtsH2/3 complex is located in the thylakoid membrane (TM), whereas the FtsH1/3 complex is located in the plasma membrane (Krynická et al., 2014; Sacharz et al., 2015). Unlike the FtsH2/3 complex, the FtsH1/3 complex is essential for *Synechocystis* viability. Recently, we have shown that FtsH1/3 is involved in the acclimation of cells to nutrient deficiency by regulating expression of genes induced under nutrient starvation (Krynická et al., 2019). Early studies demonstrated that inactivation of FtsH2, and hence the FtsH2/3 protease complex, leads to very significant phenotypic changes, such as a decrease in the level of PSI and a related decrease in chlorophyll (Chl) content in *Synechocystis* (Mann et al., 2000). However, the exact mechanism of FtsH2/3 action in biogenesis of the photosynthetic apparatus remains unknown. Although its function is only partially elucidated, there is evidence that FtsH2/3 plays a pivotal role in the quality control of PSII during biogenesis and repair in *Synechocystis* (Boehm et al., 2012; Krynická et al., 2015). The PSII complex, especially the D1 subunit, is sensitive to photo-oxidative stress, and FtsH2/3 is responsible for the selective degradation of damaged subunits (Komenda et al., 2006).

Along with FtsH2/3, high light-inducible proteins (Hlips) also participate in the maintenance of a functional PSII under stress conditions. Hlips are single-helix transmembrane proteins that are essential for the survival of cyanobacteria under various stresses, including high irradiance and low temperature (van Waasbergen et al., 2002). They are assumed to play roles in the regulation of Chl biosynthesis, non-photochemical energy quenching, and scavenging of free Chl and reactive oxygen species (ROS; for review, see Komenda and Sobotka, 2016). HliD assists in the final steps of Chl biosynthesis and recycling (Chidgey et al., 2014); moreover, all Hlips are involved in the early stages of PSII assembly. HliD and HliC protect the initial assembly of the D1/D2 intermediate complex (Knoppová et al., 2014), whereas HliA, HliB, and HliC protect CP47 and, after its attachment to the D1/D2 intermediate complex, also the downstream PSII intermediates RC47 and monomeric PSII (Yao et al., 2007; Konert et al., 2022). By binding to PSII intermediates, Hlips assist not only in biosynthesis but also in the repair of the PSII complex under stress conditions (Konert et al., 2022).

Synechocystis FtsH4 differs from the other three homologs by its occurrence as a homo-oligomeric complex (Boehm et al., 2012). Like FtsH2/3, the FtsH4 complex is located in the TM (Sacharz et al., 2015). However, details of its spatial arrangement in the TM are still unknown. Confocal microscopy of GFP-tagged FtsH4 has suggested FtsH4 distribution in spots at the distal edge of the TM adjacent to the cytoplasmic membrane under low light (LL) (Sacharz et al., 2015). By contrast, FtsH4 spots seem to be shifted inward from the outer periphery of the thylakoids after high light (HL) exposure (Sacharz et al., 2015). Because the deletion of FtsH4 has not resulted in any apparent phenotypic changes under standard conditions (Mann et al., 2000), the function of the FtsH4 complex remains to be established. The protease was recently co-isolated with D1/D2 early assembly complexes of PSII (Knoppová et al., 2022), suggesting a possible involvement of FtsH4 in the PSII assembly process.

In this work, we focus on the function and localization of the *Synechocystis* FtsH4 homolog. Using FtsH4 deletion and overexpression mutants, we demonstrate the importance of FtsH4 in acclimation to high irradiance and cold stress through dual regulation of the level of Hlips, which protect PSII assembly intermediates from photo-oxidative damage. This regulation enables sufficiently fast induction of Hlip synthesis upon a sudden increase in light intensity but also facilitates Hlip removal in response to a return to normal growth conditions or after adaptation to stress. Using microscopy techniques, we demonstrate the occurrence of fluorescently labeled FtsH4 in well-defined spots at the inner and outer periphery of the thylakoid system, which may represent PSII biogenesis centers.

RESULTS

Abundance of FtsH4 within cells compared with photosystem subunits

For the initial characterization, we determined the amount of FtsH4 protein in the cell compared with photosystem subunits. In a mass spectrometry (MS)-based proteomic analysis of TMs isolated from the wild type (WT), 1011–1066 proteins were identified at $P < 0.05$, including the abundant core photosystem subunits and FtsH4 (Supplemental Dataset 1). Using the label-free intensity-based absolute quantification (iBAQ) method, previously validated as equivalent to molar amount (Schwanhäusser et al., 2011), we determined abundance scores for FtsH4 in comparison with both photosystems (Supplemental Table 1, Supplemental Dataset 1). Interestingly, FtsH4 was approximately 50-fold less abundant than PSI components PsaA and PsaB and 20–35 times less abundant than PSII components D1 and D2 (Supplemental Table 1, Supplemental Dataset 1). Given the prevailing occurrence of FtsH4 as a hexamer, PSI as a trimer, and PSII as a dimer, one FtsH4 complex corresponds to 60–100 PSII complexes and 100 PSI complexes.

FtsH4 is not able to replace FtsH2 in the FtsH2/3 complex, nor substitute for its function in D1 degradation during high irradiance treatment

Because the previous deletion of the *ftsH4* gene had no effect on strain viability (Mann et al., 2000), the role of the FtsH4 complex in the cell remained unclear. Because *ftsH4* evolved later than other

ftsH genes (Shao et al., 2018), we tested the hypothesis that FtsH4 functionally or structurally substitutes for missing or defective FtsH2 subunits in the FtsH2/3 complex. This hypothesis has been supported by evidence that deletion of both *ftsH2* and *ftsH4*, unlike deletion of a single homolog, resulted in a non-autotrophic phenotype with a severe growth defect even under mixotrophic conditions (Supplemental Figure 1). Because our previous pulldown experiments were performed only in the presence of all other *ftsH* homologs (Boehm et al., 2012), we constructed a C-terminally FLAG-tagged derivative of FtsH4 in a strain lacking *ftsH2* (hereafter F4CF/ΔFtsH2). In this way, we tested whether FtsH4 could form a hetero-oligomeric complex with FtsH3 in the absence of FtsH2. In F4CF/ΔFtsH2, FtsH4 expression is driven exclusively by the *psbA2* promoter, resulting in its overexpression. The protein was purified from solubilized membranes using an immobilized anti-FLAG antibody. To ensure removal of non-specific or transiently interacting proteins, we increased the stringency of the affinity pulldown using additional washing steps (see methods). For initial characterization of the pulldown components, the elutions were analyzed by SDS–PAGE and clear native (CN)–PAGE (Supplemental Figure 2). After staining with Coomassie blue, the protein composition of the major bands was determined by MS. One-dimensional (1D) SDS–PAGE of the F4CF/ΔFtsH2 elution yielded three major bands of 72, 60, and 40 kDa (bands 1–3 in Supplemental Figure 2A), all of which belonged to FtsH4 and its degradation products, confirming the purity of the F4CF/ΔFtsH2 preparation (Supplemental Table 2). CN–PAGE separation of the elution resulted in three major complexes corresponding to 600, 820, and 900 kDa (Supplemental Figure 2B). Proteins present in each complex were quantified by MS as above. As expected, FtsH4 was the major protein component in all complexes, whereas the proportions of FtsH1 and FtsH3 were in the range of 0.02%–0.08% and 0.13%–0.22% of FtsH4, respectively (Supplemental Table 3, Supplemental Dataset 2), indicating the presence of the FtsH1/3 complex most probably as a non-specific contaminant. The very low abundance of FtsH3 relative to FtsH4 excluded the possibility of FtsH4 replacing FtsH2 within the FtsH2/3 hetero-complex and strongly supported the exclusive formation of the homo-hexameric FtsH4 complex (Boehm et al., 2012).

Although FtsH4 appears not to have been incorporated into the hetero-oligomeric complex with FtsH3 in the absence of FtsH2, an outstanding question is whether the homo-hexameric FtsH4 complex might functionally substitute for the FtsH2/3 complex in its role in PSII repair under high irradiance. Therefore, the F4CF/ΔFtsH2 strain was used to determine whether the surplus of FtsH4 can compensate for the lack of FtsH2. We analyzed the ability of F4CF/ΔFtsH2 to respond to high irradiance at 500 μmol photons m^{-2} s^{-1} (hereafter HL) by efficiently degrading D1 and D2. Both F4CF/ΔFtsH2 and ΔFtsH2, used as a control, were exposed to HL in the absence or presence of the protein synthesis inhibitor lincomycin (LIN). Immunoblotting confirmed the previously observed inhibition of D1 and D2 degradation caused by the absence of FtsH2/3 (Komenda et al., 2006) (Supplemental Figure 3, blue rectangle), which was reflected in the slow disappearance and high smearing of the D1 and D2 bands because of their photo-oxidative damage. This smearing was slightly more pronounced in the presence of LIN (Supplemental Figure 3, blue rectangle) compared with the absence of LIN (Supplemental Figure 3, red rectangle), suggesting that active protein synthesis at least partially limited photodamage. In the double mutant, smearing of the D1 and D2 signals was less pronounced when compared with the single ΔFtsH2 mutant, although the disappearance of the bands was still slow. These results showed that the surplus of FtsH4 did not restore D1 and D2 degradation but did limit photo-oxidation of these proteins. Likewise, deletion of *ftsH4* in the ΔFtsH4 mutant did not affect D1 turnover during HL stress. D1 degradation was comparable with WT levels (Supplemental Figure 4). These results indicate that FtsH4 does not play any role in PSII repair and hence does not substitute for the function of FtsH2/3. However, FtsH4 overproduction might contribute to *de novo* synthesis/photoprotection of D1 and D2, leading to higher vitality of the strain in the ΔFtsH2 background (Supplemental Figure 3).

ΔFtsH4 cells contain more PSI trimers and are sensitive to HL stress

Deletion of *ftsH4* had no obvious negative impact on growth under normal light (NL; 40 μmol photons m^{-2} s^{-1}) or LL (5 μmol photons m^{-2} s^{-1}; Supplemental Figure 1). In fact, growth of the ΔFtsH4 mutant appeared faster under these conditions in comparison with WT. The probable cause of this effect was a statistically significant higher level of Chl per cell compared with WT, i.e., 120%, $P = 0.002$ (Figure 1A). This extra Chl was apparently incorporated into the PSI trimer (PSI(3)), which was surplus in ΔFtsH4 compared with WT (Figure 1B).

However, when cells of both strains were exposed to HL, the growth of ΔFtsH4 was strongly retarded compared with that of WT (Supplemental Figure 5A). The distinct effect of HL treatment was also apparent from the whole-cell absorption spectra reflecting major cellular pigment content per optical density at 750 nm (OD_{750nm}). This content decreased more in WT than in the mutant (Supplemental Figure 5C). To identify differences elicited by HL in the photosynthetic apparatus of WT and mutant cells, we analyzed membranes isolated from cells exposed to HL by CN–PAGE (Figure 1). CN–PAGE confirmed that the levels of PSI(3) and PSII dimer (PSII(2)) were maintained for longer in the mutant compared with WT (Figure 1C and 1D). Moreover, two-dimensional (2D) gel analysis of membranes revealed a higher accumulation of Hlips, namely, HliA/B and HliD, in ΔFtsH4 compared with WT (Figure 1E, blue rectangles). A similar effect was observed when ΔFtsH4 was exposed to cold stress under increased light intensity. Nine days of exposure to 18°C and irradiance of 160 μmol photons m^{-2} s^{-1} (hereafter cold stress) caused growth retardation in the mutant compared with the control (Supplemental Figure 5B). As in the case of HL stress, 2D gel analysis revealed an accumulation of unassembled HliD and HliA/B in ΔFtsH4 analyzed after 5 days of cold stress (Figure 1F, blue rectangles).

Over the course of HL stress, WT cells exhibited an inverse regulation of FtsH4 and HliD protein levels. Whereas the level of HliD increased within 24 h of HL, the level of FtsH4 decreased (Figure 1G). In ΔFtsH4, the HliD level was even higher than in WT after HL treatment (Figure 1G). Quite the opposite effect was observed in the F4CF mutant overexpressing FtsH4. The level of HliD protein was lower compared with the control A3 strain (Metz et al., 1989) after 24 h of HL (Figure 1H).

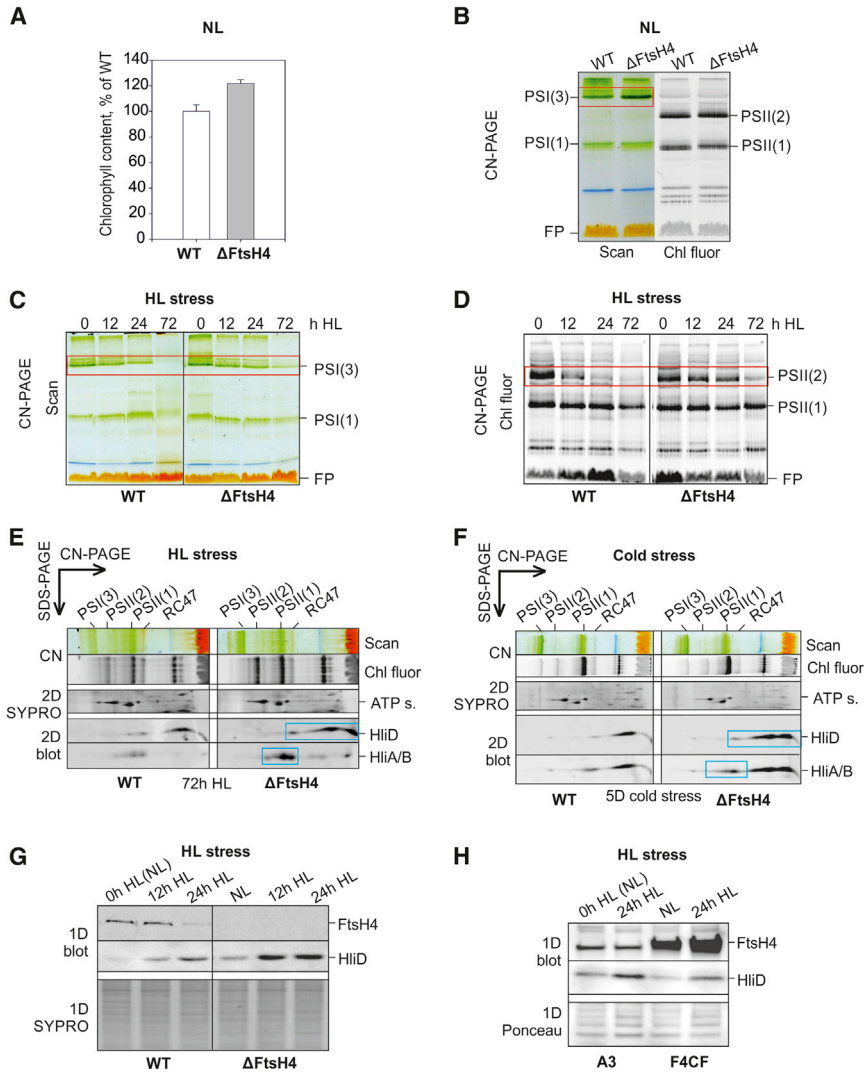

Figure 1. Characterization of WT and FtsH4 mutants under various conditions.

(A) Relative chlorophyll (Chl) content in WT and ΔFtsH4 cells grown under normal light (NL; 40 μmol photons m^{-2} s^{-1}/28°C; exponential growth phase OD_{750nm} of 1), expressed as a percentage of Chl levels of the WT control. Chl content was quantified per OD_{750nm} of 1, mean of six measurements, $P = 0.002$ (*t* test).

(B–D) Membrane protein complexes in WT and ΔFtsH4 cells under NL **(B)** or after 0, 12, 24, and 72 h of HL exposure (500 μmol photons m^{-2} s^{-1}) **(C and D)** were analyzed using CN–PAGE, with loadings matched by OD_{750nm}; the gel was scanned in white light (Scan; B and C) and for Chl fluorescence (Chl fluor; B and D); designation of complexes: free pigments [FPs]; PSI(1) and PSI(3): monomeric and trimeric photosystem I; PSII(1) and PSII(2): monomeric and dimeric photosystem II; note differences in levels of PSI(3) or PSII(2) (red rectangles).

(E and F) Membrane protein complexes in WT and ΔFtsH4 cells after 72 h of HL **(E)** or 5 days (5D) of cold stress (160 μmol photons m^{-2} s^{-1}/18°C) **(F)** were analyzed using CN–PAGE followed by the second dimension SDS–PAGE with HliD, and HliA/B detection using specific antibodies (2D blot); designation of complexes: ATP s., α/β subunits of ATP synthase; RC47, PSII monomer lacking CP43 antenna; othersas in **(A)–(C)**; note differences in levels of Hlips (blue rectangles).

(G and H) 1D SDS–PAGE/immunoblot analysis of proteins in membranes isolated from WT and ΔFtsH4 cells **(G)** and from cells of the control *psbA2* deletion (A3) and FtsH4-overexpressing (F4CF) strains **(H)** before and after HL exposure; specific antibodies for FtsH4 and HliD were used for immunodetection; sections of the SYPRO-stained gel **(G)** and Ponceau-stained blot **(H)** are shown to document equal loading of the samples based on OD_{750nm}.

Detrimental effect of HL treatment on the ΔFtsH4 mutant in the stationary growth phase

Another inverse regulation of FtsH4 and HliD protein was observed after reaching the stationary phase (SP), but in the opposite direction than in HL. In WT growing at NL, the HliD protein content decreased, whereas that of FtsH4 increased, after the transition from exponential phase to SP. By contrast, in the ΔFtsH4 mutant, HliD protein remained accumulated (Figure 2A). Unfortunately, we could not compare the levels of other Hlips because they were undetectable under these conditions.

During growth at NL, the ΔFtsH4 mutant reached SP at slightly lower OD_{750nm} than WT (Supplemental Figure 6). Except for this observation, we did not detect any significant difference between the vitality of WT and ΔFtsH4 cells at NL. By contrast, a severe growth defect was observed when the ΔFtsH4 cells were exposed to HL after reaching SP (hereafter HLsp). When cells of WT and ΔFtsH4 were diluted and exposed to HL, the growth of ΔFtsH4 was significantly retarded compared with that of WT. After 48 h of such treatment, the ΔFtsH4 culture reached only 40% of the WT OD_{750nm}, and it lost pigments (Figure 2B). Interestingly, as in the previous HL experiments, 1D protein analysis revealed a pronounced accumulation of HliD in ΔFtsH4 under these conditions (Figure 2A). The most drastic effect on ΔFtsH4 viability was exerted by a combination of HL and cold stress after dilution of the SP culture (HLsp/cold). Unlike WT, the mutant repeatedly died within 24 h (Figure 2C). Within the first 12 h of stress, levels of Chl and phycobilins in ΔFtsH4 declined much more slowly, similarly to HL stress. However, after 24 h, we observed a sharp drop in the contents of all pigments, signifying incipient cell death (Figure 2C).

Growth retardation of ΔFtsH4 after exposure to HL, which was even more pronounced when the cells were diluted from SP, indicated problems with acclimation to HL stress.

FtsH4 regulates fast Hlip induction and degradation

Protein analysis of long-term (24 or 72 h) HL-treated cells revealed differences in Hlip accumulation in WT and ΔFtsH4. We also observed a difference in fast Hlip inducibility by HL and in subsequent Hlip disappearance after a shift from HL to NL. Although the signal of Hlips in WT was the most intense after

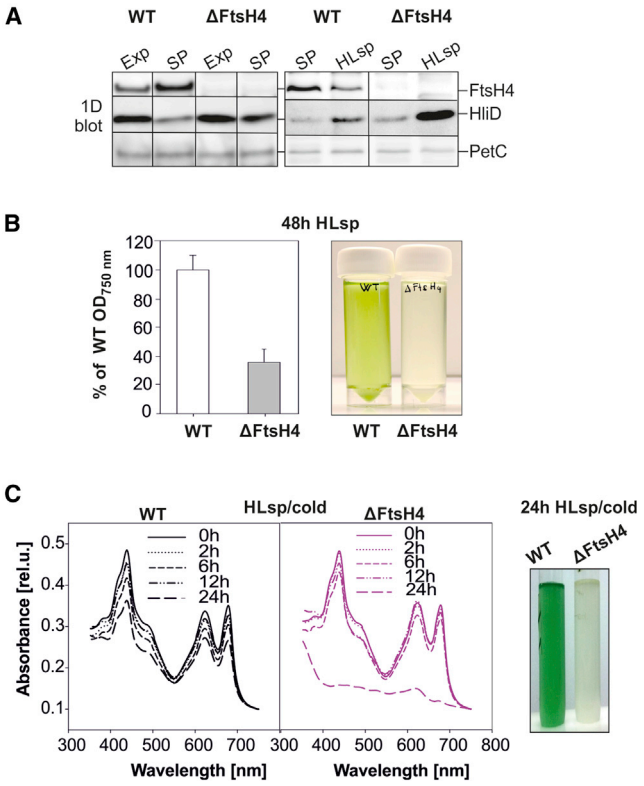

Figure 2. Effect of HL on WT and ΔFtsH4 cells diluted from stationary phase (SP).

(A) 1D SDS–PAGE/immunoblot analysis of membrane protein complexes isolated from WT and ΔFtsH4 cells in Exp or SP growth and treated with HL (500 μmol photons m^{-2} s^{-1}/28°C) after dilution from SP to OD_{750nm} 0.05 (HLsp). Antibodies specific to FtsH4, HliD, and PetC were used for immunodetection, with the PetC signal used to document equal loading of the samples based on the same OD_{750nm}.

(B) Growth and photograph of WT and ΔFtsH4 cells after 48 h of HLsp. The OD_{750nm} of both cultures was expressed as a percentage of the WT values. Values are means of four biological replicates ± SD. $P = 0.006$.

(C) Whole-cell absorption spectra of WT and ΔFtsH4 diluted from SP to OD_{750nm} 0.05 and treated at 500 μmol photons m^{-2} s^{-1}/18°C (HLsp/cold) for 0, 2, 6, 12, and 24 h. Cell cultures were photographed after cultivation for 24 h under HLsp/cold.

2 h of HL and continuously decreased after the shift to NL, Hlip induction in the ΔFtsH4 mutant was much lower, and subsequent degradation was delayed. The highest accumulation of HliA/B and HliD was reached 1 h after termination of HL, and it did not reach WT levels. Then the levels slightly decreased. By contrast, HliC accumulated to the highest level even 2 h after the termination of HL (Supplemental Figure 7).

To determine in more detail how FtsH4 affects Hlip inducibility, we measured the level of Hlip biosynthesis by radiolabeling. The 2D autoradiogram of proteins from *ftsH4* deletion (ΔFtsH4) and FtsH4 overexpression (F4CF) mutants treated with HL for 30 min showed that overall Hlip biosynthesis was downregulated in the ΔFtsH4 mutant, whereas it was significantly enhanced in F4CF compared with WT and A3, respectively (Figure 3). A similar downregulation was observed for FtsH2 and large subunits of PSII such as D1, D2, CP43, and CP47. The analysis of Hlip transcripts after 30 min of HL exposure (the same conditions used for the autoradiogram) confirmed the results of radioactive labeling: downregulation of *hlip* and *ftsH2* transcripts in the ΔFtsH4 mutant and their upregulation in F4CF (Supplemental Table 4). By contrast, the expression of *psaA*, which was attenuated in WT during acclimation to HL, was upregulated in ΔFtsH4 and downregulated in F4CF. These results suggest that FtsH4 regulates, most probably indirectly, the transcription process or transcript stability of Hlips, FtsH2, D1, and PsaA/B.

Paradoxically, in the ΔFtsH4 mutant, despite its slower inducibility, we observed an accumulation of Hlips after long-term HL exposure (Figure 1E). To further test the effect of FtsH4 deletion on Hlips accumulation, we employed PSI knockout mutants (ΔPSI). The ΔPSI strain maintains Hlips at a detectable level even at NL (Funk and Vermaas, 1999), and we wanted to demonstrate that lack of FtsH4 would lead to the accumulation of Hlips independently of light conditions. Notably, 2D gel analysis of ΔPSI or the ΔPSI/ΔFtsH4 double mutant revealed significantly higher levels of all Hlips in the double mutant (Supplemental Figure 8).

Overall, the results indicated that FtsH4 regulates Hlips at both the transcript and the protein level, and that Hlips, especially HliD and HliA/B, might be potential substrates for FtsH4 degradation.

Hlips are directly degraded by FtsH4 *in vitro*

To demonstrate that the regulation of Hlip levels is at least partly a direct effect and that FtsH4 is able to digest these proteins, we performed an *in vitro* assay of FtsH4 proteolytic activity according to Tomoyasu et al. (1995), using purified His-tagged FtsH4 produced in *Synechocystis* as an active form of the enzyme. In the negative control, protease activity was inhibited using a commercially available cocktail supplemented with EDTA. As a second negative control, we used a His-tagged FtsH4 derivative inactivated by the point mutation D515N in the protease domain. Purified His-tagged Hlips produced in *Synechocystis* were used as FtsH4 substrates. Besides Hlips, we also assessed the ability of FtsH4 to degrade Sll1106, a protein of unknown function.

Figure 4 shows that after a 3-h reaction, the amounts of HliA, HliB, and HliD decreased by 50%–60% in the presence of the active variant of FtsH4 (Figure 4, lane 1). In the case of HliC, the decline was even more pronounced, reaching 90%. As expected, Hlip levels were not reduced in either of the negative controls (Figure 4, lanes 2 and 4). By contrast, the level of Sll1106 was not reduced in the presence of the active enzyme, demonstrating that this uncharacterized protein is not an FtsH4 substrate *in vitro*. In addition, the active FtsH variant exhibited low stability during the reaction (Figure 4, lanes 1 and 3), whereas both inactive and active variants were stable in the presence of protease inhibitor (Figure 4, lanes 2 and 4). We therefore suggest that FtsH4 is susceptible to autoproteolysis.

FtsH4 co-purifies with Sll1106

To identify proteins interacting with FtsH4, we constructed a strain expressing a C-terminally FLAG-tagged derivative of FtsH4 (F4CF) also in the WT background. As in F4CF/ΔFtsH2, FtsH4 expression in F4CF is driven exclusively by the *psbA2*

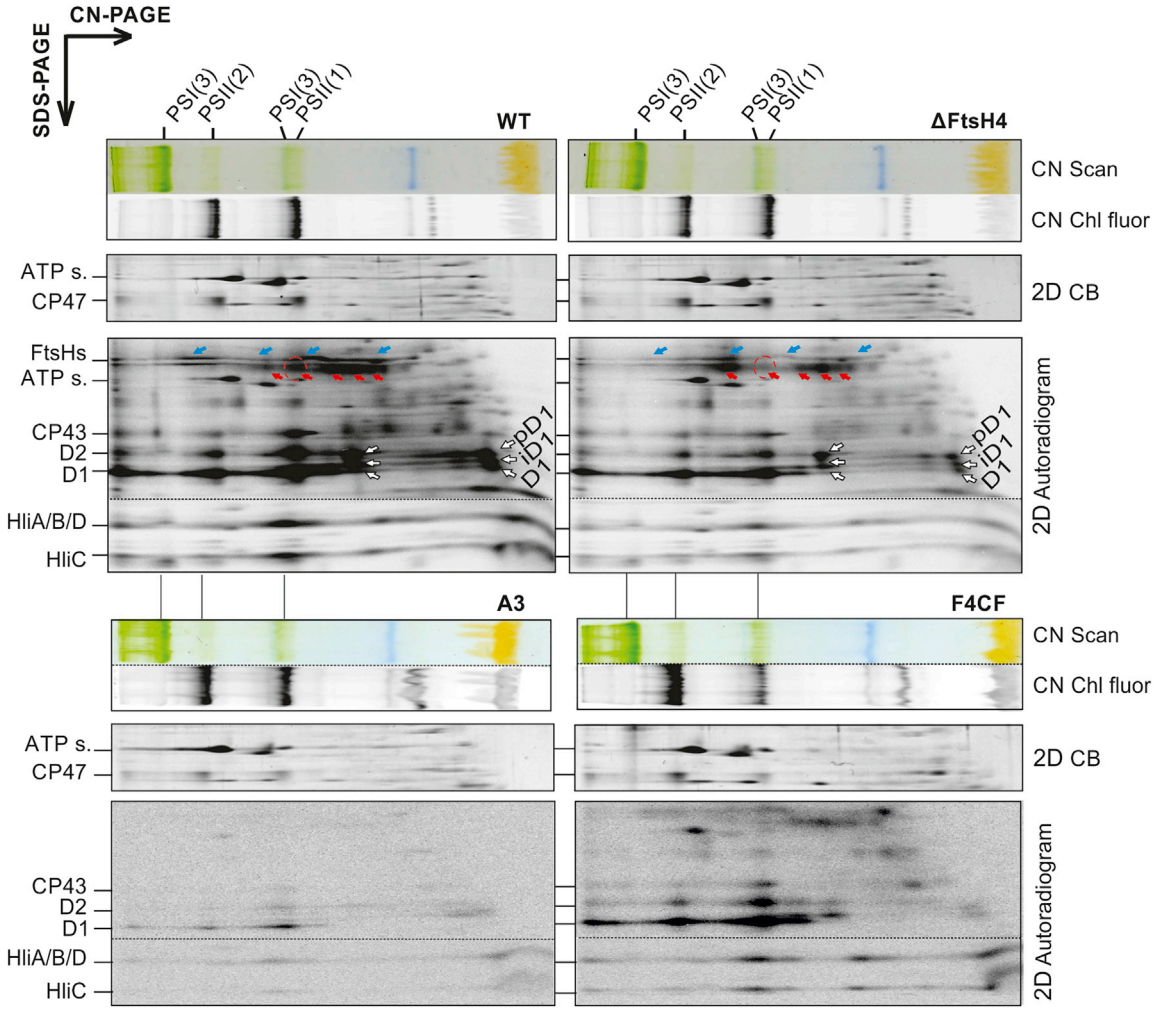

Figure 3. *De novo* synthesis of membrane proteins in WT, ΔFtsH4, A3, and F4CF strains.

Membranes isolated from radiolabeled cells of WT, ΔFtsH4, A3 (control *psbA2* deletion strain), and F4CF were analyzed by 2D CN/SDS–PAGE. The CN gel was scanned in white light (Scan) and for chlorophyll fluorescence (Chl fluor). The 2D gels were stained with Coomassie blue (CB) and developed overnight in a phosphoimager (Autoradiogram). Complexes are designated as in Figure 1. Individual PSI or FtsH complexes are marked by red and blue arrows, respectively. Position of PSI(1) is indicated by a red dashed circle. Samples were loaded on the same OD_{750nm} basis. Sections of CB-stained gels are shown to document equal loading of the samples. ATP s., α/β subunits of ATP synthase.

promoter, resulting in its overexpression. The protein was purified from solubilized membranes using an immobilized anti-FLAG antibody and analyzed by MS (Supplemental Dataset 3). WT membranes were used as a negative control for detection of non-specifically purified proteins (Supplemental Dataset 3). As expected, FtsH4 was the most abundant protein in the F4CF elution. In addition, the uncharacterized protein Sll1106, HofG (PilA1), CurT (Slr0483), the PSI reaction center subunit PsaD, and the PSII core antenna subunit CP47 were among the most abundant proteins specifically co-purified with FtsH4 (Supplemental Table 5, Supplemental Dataset 3). Quantification by the MS-based iBAQ method revealed that the mean abundance score for Sll1106 was only 4-fold lower than that of FtsH4, whereas the scores for the other proteins were >15-fold lower. This apparent enrichment of Sll1106 suggests that this membrane protein, with a molecular mass of 18 kDa, may be a component of a complex with FtsH4. By contrast, the other proteins in the five most abundant groups probably represent co-localized membrane components. The F4CF pulldown was also analyzed by 1D and 2D SDS–PAGE, with both Coomassie blue staining and immunodetection (Figure 5). Comparison of the stained and immunodetected intensities in both 1D and 2D gels confirmed FtsH4 as the major protein in the F4CF eluate. Immunodetection also revealed several degradation products of FtsH4 protein, indicating probable autoproteolysis. The second most intense signal in the stained gel corresponded to Sll1106, consistent with the MS results. The 2D gel analysis supports our hypothesis that Sll1106 is a real component of the FtsH4 complex because the major fraction of Sll1106 co-migrated in the native gel with two larger FtsH4 complexes (Figure 5). Accordingly, a fraction of Sll1106 was also detected in all three CN-separated complexes of the F4CF/ΔFtsH2 preparation (Supplemental Dataset 2). The fact that Sll1106 was not degraded by FtsH4 *in vitro* (Figure 4) only strengthens the idea of this protein as a direct binding partner of the FtsH4 complex.

A

Reagents	1	2	3	4	5	6	7	
FtsH4	act	in	act	mut	—	—	—	
EDTA Inhib.	—	+	—	—	—	—	—	
substrate	100	100	—	100	100	50	25	%

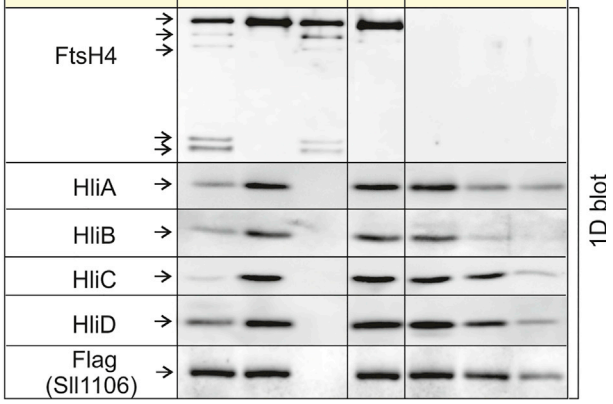

B

Substrate quantification after 3h reaction			
substrate	FtsH		
	act	in	mut
HliA	40 ± 5	102 ± 36	118 ± 26
HliB	51 ± 11	99 ± 9	96 ± 6
HliC	8 ± 0	92 ± 2	101 ± 8
HliD	45 ± 6	100 ± 2	107 ± 12
Sll1106	99 ± 8	106 ± 34	112 ± 5

Figure 4. FtsH4 proteolytic assay *in vitro*.

(A) Hlips, Sll1106, and FtsH4 variants were isolated from membranes of *Synechocystis* strains expressing His-tagged (FtsHs and Hlips) or Flag-tagged (Sll1106) protein derivatives as described in methods. Reagents used in individual reactions 1–7 are presented in the table above the blot. At the start of the reaction, samples 1–4 contained 0.3 μg of FtsH4 protein in total. Samples 1/2 and 4/5 contained 0.2 μg of the substrate (Hlips or Sll1106, respectively), corresponding to 100% in calibration. Samples 1–3 contained the active variant of FtsH4 (act). Sample 2 was supplemented with protease inhibitor cocktail containing EDTA to inhibit activity of the FtsH protease (in). Sample 4 contained inactive FtsH4 variant (mut). Composition of the reaction buffer: 25 mM MES (pH 6.5), 5% glycerol, 2 mM Mg^{2+}, 2 mM Ca^{2+}, 0.4 μM Zn^{2+}, and 3 mM ATP. All samples were incubated for 3 h at 37°C. After incubation, the samples were denatured by 1% SDS and analyzed by 1D SDS–PAGE. The protein bands were electroblotted to polyvinylidene fluoride; the presence of substrates and FtsH4 was detected by specific antibodies, and Sll1106-FLAG was detected by FLAG antibody.

(B) Substrate quantification: the percentage of the substrate in a particular reaction sample relates to the initial substrate amount (100%); values are means of three measurements of three independent reactions ± standard deviation. Quantification of bands was performed with ImageQuant TL software (GE Healthcare, Uppsala, Sweden).

Patchy localization of FtsH4 within the TM

Previous studies have shown that FtsH4, like FtsH2/3, is located in the TM (Boehm et al., 2012; Sacharz et al., 2015). Whereas the FtsH2 signal more or less overlapped with that of Chl, which mostly originates from fully assembled PSII complexes, the FtsH4 signal appeared to be shifted to the distal edge of the TM closer to the cytoplasmic membrane (Sacharz et al., 2015). To further explore the localization of the thylakoid FtsHs, we analyzed GFP-tagged FtsH2 and FtsH4 derivatives by structured illumination microscopy (SIM), achieving a higher resolution than that obtained by confocal microscopy. SIM of the GFP-tagged FtsH2 derivative (hereafter FtsH2-GFP) confirmed that FtsH2 is located entirely in the TM. Its signal was diffuse throughout the membrane, with areas of higher intensity, and largely overlapped with Chl autofluorescence (Supplemental Figure 9) (Krynická et al., 2014; Sacharz et al., 2015). By contrast, the signal of the GFP-tagged FtsH4 derivative (hereafter FtsH4–GFP) was solely concentrated in well-defined membrane clusters resembling "blobs" or occasionally "tunnels" instead of being distributed regularly within the whole TM of *Synechocystis* (Figure 6A). The 2D SIM analysis showed that cells contained distinct spots slightly protruding above a low continuous background in the TM. Interestingly, when comparing the FtsH4–GFP and Chl fluorescence signals within the same cells, the GFP signal, although localized to the TM, was slightly shifted toward the inner and outer periphery of the TM compared with the Chl signal (see Figure 6A). Three-dimensional (3D) views rendered by both confocal microscopy and SIM confirmed this punctate pattern and illustrated the inhomogeneous distribution of FtsH4–GFP in the cell (Figure 6B). For the confocal microscopy 3D image, we combined three fluorescent signals from GFP, PSII-associated Chl, and phycobilins. Consistent with the 2D SIM analysis, the GFP signal mostly did not overlap with the phycobilin and Chl signals. It has previously been shown that pigment proteins are not uniformly distributed along the TM (Casella et al., 2017). They form photosynthetic microdomains, specific membrane areas with a diameter ranging from 0.2 to 1 μm defined by co-localization of photosystems (PSI and PSII) and phycobilisomes (PBSs) (Strašková et al., 2019). Our results indicate that FtsH4–GFP blobs are situated outside of the Chl/phycobilin-abundant areas of microdomains.

To study the location of FtsH4 under different conditions, we exposed the FtsH4–GFP cells to HL for 24 h or LL for 72 h and compared them with NL-grown cells in an exponential growth phase or SP. In Supplemental Figure 10, all images have been scaled to the same intensity range as the NL sample. Calculations of mean GFP intensity in each of the four conditions (n = 56) gave values of 716 ± 85 (HL), 761 ± 73 (NL), 866 ± 127 (LL), and 912 ± 90 (SP), demonstrating an increase in FtsH4–GFP abundance with decreasing light intensity. The decrease in FtsH4 signal in HL and its increase in SP cells compared with NL cells were consistent with FtsH4 immunodetection in Figures 1G and 2A. Besides the total FtsH4–GFP levels, the most apparent difference among cells from different conditions was the number of clusters (blobs) indicating inhomogeneity in the FtsH4–GFP location within the TM. The inhomogeneity was quantified by taking the log-transformed mean-normalized standard deviations of the fluorescence signal over pixels corresponding to the thylakoid zones. The number of clusters increased in the order of HL < NL/LL < SP (−0.92 ± 0.12 [HL], −0.76 ± 0.19 [NL], −0.75 ± 0.2 [LL], −0.37 ± 0.22 [SP]), demonstrating the lowest inhomogeneity in HL and the highest in SP (Supplemental Figure 11).

DISCUSSION

The role of the FtsH4 protease in cyanobacteria has remained elusive since the description of the *ftsh4* gene and the FtsH4-less strain, which did not exhibit any obvious phenotypic

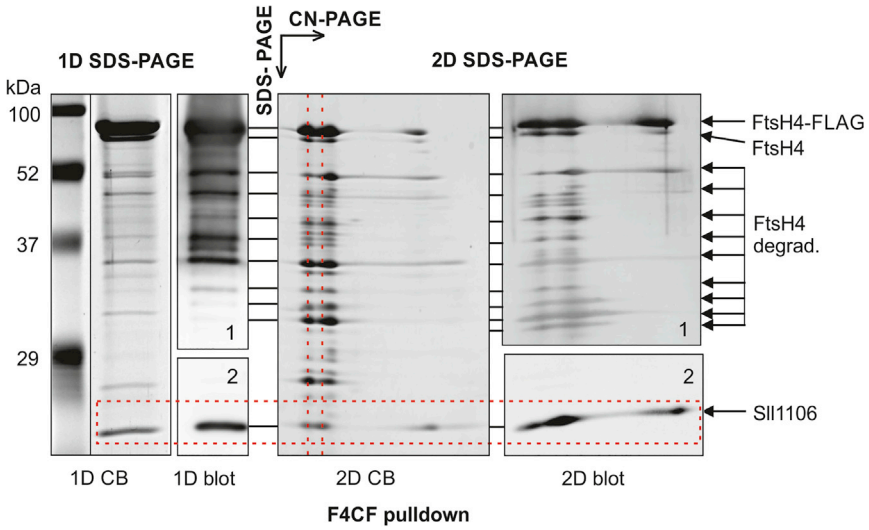

Figure 5. Analysis of FLAG-tagged FtsH4 (F4CF) pulldown by 1D and 2D SDS–PAGE.
A total of 20 μl of elution was loaded on both 1D SDS and CN gels, and the CN strip was then separated on the 2D SDS gel. 1D and 2D SDS gels were stained with Coomassie blue (1D, 2D CB) or used for immunodetection (1D, 2D blot). Blots were probed with antibodies specific for FtsH4 and Sll1106 in boxes 1 and 2, respectively. FtsH4 degrad. are putative degradation products of the FtsH4 protease, probably resulting from autoproteolysis. The red dashed rectangle indicates the position of Sll1106. Red dashed lines indicate co-migration of Sll1106 with FtsH4 complexes.

distinctions from WT under standard growth conditions (Mann et al., 2000). Nevertheless, transcriptional analysis has previously shown overexpression of the *ftsH4* gene under stress conditions such as HL, SP, and nutrient depletion (Kopf et al., 2014). Our results excluded the possibility that FtsH4 structurally and functionally substitutes for the missing or nonfunctional FtsH2 subunit in the FtsH2/3 complex. In agreement with this conclusion, a surplus of FtsH4 in the ΔFtsH2 background did not contribute to D1 degradation after exposure to HL (Supplemental Figure 3), and the FtsH4-less strain was able to degrade D1 comparably with the WT (Supplemental Figure 4). Instead, our results indicate that FtsH4 functions in acclimation to different stresses such as HL, cold stress, and even the SP via regulating the level of Hlips. In general, the response of *Synechocystis* to various stresses involves induction of Hlips (van Waasbergen et al., 2002). By scavenging free Chl and ROS generated by stress conditions, Hlips are involved in the protection of PSII assembly and repair processes (for review, see Komenda and Sobotka, 2016). After acclimation to stress or after resumption of optimal growth conditions, the cells gradually degrade Hlips, but to date no protease has been ascribed to this process. The evidence presented here suggests that FtsH4 fulfills this role.

The FtsH4-less strain exhibited accumulation of HliD, HliA/B, and eventually HliC, especially under conditions where *de novo* Hlip synthesis was attenuated, such as SP, recovery from HL, or long-term HL exposure (24 or 72 h). In WT cells, we observed an inverse regulation of FtsH4 and HliD levels (Figure 1G). After the cells reached SP, the HliD level decreased, whereas the FtsH4 level increased (Figure 2A). Unlike in WT, the level of HliD was stabilized in the FtsH4-less strain in SP. Conversely, under HL, the level of HliA/B and HliD increased significantly in WT, whereas the level of FtsH4 decreased. Theoretically, if the FtsH4 protease plays a role in HliD and HliA/B degradation, its gradual decrease under HL would be logical because maintenance of a high Hlip level is necessary for photoprotection of PSII assembly intermediates and apparatus, which assists in PSII biogenesis. The key role of FtsH4 in Hlips degradation is also supported by the phenotype of the FtsH4 overexpression mutant, in which the level of Hlips was reduced more than in WT (Figure 1H). Finally, the *in vitro* proteolytic assay demonstrated that all purified Hlips were digested by the active form of the FtsH4 complex, whereas the inactive form had no effect. Thus, we suggest HliA-D as substrates of the FtsH4 protease.

Our results demonstrate that FtsH4 also affects Hlip inducibility during HL stress. Whereas Hlip expression was downregulated in the ΔFtsH4 mutant, we observed strong upregulation in the mutant overexpressing FtsH4 (Supplemental Table 4). In cyanobacteria, Hlip expression induced by HL and/or cold stress is regulated by a two-component system consisting of Hik33/NblS (DspA) kinase and the RpaB response regulator (reviewed in Los et al., 2010; Rachedi et al., 2020). The Hik33 kinase is involved in perception of HL stress. Under normal conditions, RpaB is phosphorylated by Hik33 and represses HL-inducible genes while activating the expression of genes for PSI and PBS components (Riediger et al., 2019). RpaB phosphorylation by Hik33 is inhibited, and the binding affinity of RpaB to DNA is temporarily diminished shortly after HL exposure (Lopez-Redondo et al., 2010; Yasuda et al., 2020). As a consequence, the HL-inducible genes encoding Hlips, PSII subunits D1 and D2, FtsH2, and several others, including the SrrA regulatory protein, are induced. Simultaneously, expression of genes for PSI and PBS is suppressed (Riediger et al., 2018, 2019). After acclimation to HL, Hik33 regains kinase activity, but RpaB remains partially phosphorylated because of competition with the SrrA regulator (Lopez-Redondo et al., 2010). This results in weak expression of both Hlips and PSI/PBS (Figure 7A).

Subdued response to HL stress because of the lack of FtsH4 protease was also evident from whole-cell absorption spectra. ΔFtsH4 exhibited a slower decrease in Chl and phycobilin content during 24 h of acclimation to HL compared with the WT (Supplemental Figure 5C). We do not expect FtsH4 to regulate the expression of Hlips and PSI/PBS directly. By contrast, our results imply that FtsH4 protease has a role in regulation of the Hik33–RpaB response to HL stress. However, the mechanism by which FtsH4 might regulate the response remains unexplained. FtsH4 might control the level of a negative regulator of HL-induced genes, such as RpaB or potentially SipA, which stimulates Hik33 kinase activity and hence RpaB phosphorylation

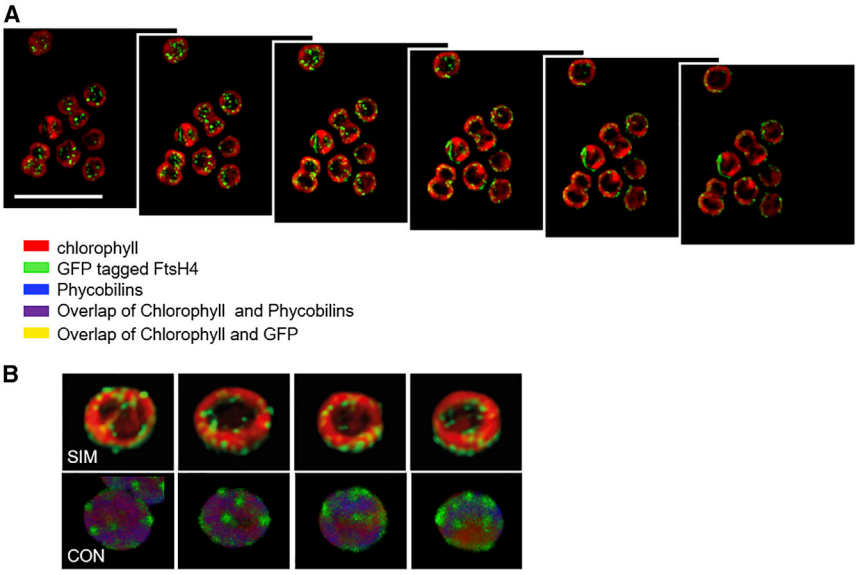

Figure 6. Localization of GFP-tagged FtsH4, Chl, and phycobilins in *Synechocystis* cells.

(A) Structured illumination microscopy (SIM) of FtsH4–GFP. Axial slices of *Synechocystis* cells with GFP are in green and Chl in red. The axial slices are 125 nm apart, and the scale bar represents 5 μm.

(B) 3D images obtained using SIM and 3D confocal microscopy (CON). The SIM 3D image was obtained using 2D axial slices 125 nm apart, and 3D confocal microscopy images were obtained using 15 2D slices with a thickness of 150 nm.

(Sakayori et al., 2009), similar to FtsH1/3 regulation of the level of Fur, NdhR, or PhoU repressors under nutrient starvation. In the absence of FtsH4, the level of the negative regulator increases, resulting in inhibition of the stress response (Krynická et al., 2019). Nevertheless, we cannot exclude the possibility that FtsH4 affects the function of sigma factors involved in the HL stress response. As discussed in Srivastava et al. (2020), group 2 σ factors SigD (Sll2012) and SigE (Sll1689) activate the expression of HL-induced photosynthetic genes.

The overall phenotype of the FtsH4-less strain showed that FtsH4 plays an important role in the acclimation to HL. This acclimation in WT is manifested by a continuous reduction in levels of photosystems, especially PSI, and their antennas (see also Kopečná et al., 2012). This reduction protects the cell from overexcitation and production of ROS. In an FtsH4-less mutant, PSI and PBS were maintained for a much longer time, probably resulting from an ineffective Hik33–RpaB response. Besides PSI/PBS, the FtsH4-less mutant also unnecessarily stabilized the level of PSII via overaccumulation of HliD and HliA/B after long-term HL exposure. HliD accumulation in ΔFtsH4 might also explain the higher Chl levels in this mutant because HliD is involved in the final steps of Chl biosynthesis (Chidgey et al., 2014), and newly synthesized Chl is preferentially channeled into PSI(3) (Kopečná et al., 2012). At low temperature, ROS production also increases because electron flux into the Calvin cycle declines owing to a decrease in the activity of ribulose-1,5-bisphosphate carboxylase/oxygenase, and consequently, photosynthetic electron transport becomes over-reduced (Allen and Ort, 2001; Biswal et al., 2011). When combined with low temperature, the adverse effect of HL on cells is multiplied, and the absence of FtsH4 becomes lethal. The enhanced adverse effect of HL in the FtsH4-less mutant also occurs when cells are exposed to stress after reaching SP. Most biochemical processes are attenuated in SP, and subsequent dilution and HL exposure require a rapid and efficient re-start, including initiation of photosynthetic gene expression, driven mainly by the Hik33–RpaB transduction pathway under HL/cold stress (Rachedi et al., 2020). Our findings demonstrate that *Synechocystis* FtsH4 is involved in adapting to HL stress by dual regulation of Hlip levels (Figure 7A). On one hand, it positively regulates rapid Hlip expression after a shift to stress conditions, probably by activating the Hik33–RpaB pathway. On the other hand, it negatively regulates Hlips at the protein level under conditions where a high concentration of Hlips is no longer needed.

The role of FtsH4 in regulation of the level of Hlips corresponds well with the fact that FtsH4 was co-purified with several PSII subunits (Supplemental Table 5, Supplemental Dataset S3), preferentially with the CP47 antenna, which is protected by HliA/B/C during its assembly within PSII (Konert et al., 2022). In addition to CP47, Sll1106, CurT, and PilA1 proteins were among the most abundant proteins in the F4CF pulldown. Because the levels of most co-purified proteins were low in comparison with FtsH4, we suggest co-localization rather than attachment to the FtsH4 complex. The only exception seems to be Sll1106, a protein of unknown function, which was highly enriched in the pulldown and could be considered the true binding partner of FtsH4. Both Sll1106 and FtsH4 were previously found in the pulldown of protoporphyrinogen oxidase HemJ (Skotnicová et al., 2018), the enzyme catalyzing the reaction that yields protoporphyrin IX, the last common precursor of heme and Chl biosynthesis. Moreover, FtsH4, together with Sll1106, CurT, and PilA1, was recently identified in association with D1/D2 assembly intermediates isolated using PsbI–FLAG from a strain lacking CP47 (Knoppová et al., 2022) (Figure 7B).

The biogenesis of photosynthetic complexes is coordinated in parallel with pigment synthesis and insertion of Chl into their apoproteins. Hlips generally operate at the interface between the last steps of Chl biosynthesis/recycling and the biogenesis of Chl-binding proteins of PSII. It has been suggested that PSII assembly takes place in specialized CurT-enriched membrane regions within the TM near the plasma membrane (Rast et al., 2019). Potential contact sites between the TM and plasma membrane and involvement of so-called thylakoid centers have been discussed in relation to this process (Stengel et al., 2012).

Using GFP-tagged FtsH4, we found that FtsH4 complexes, unlike the other FtsH homologs, are concentrated in well-defined

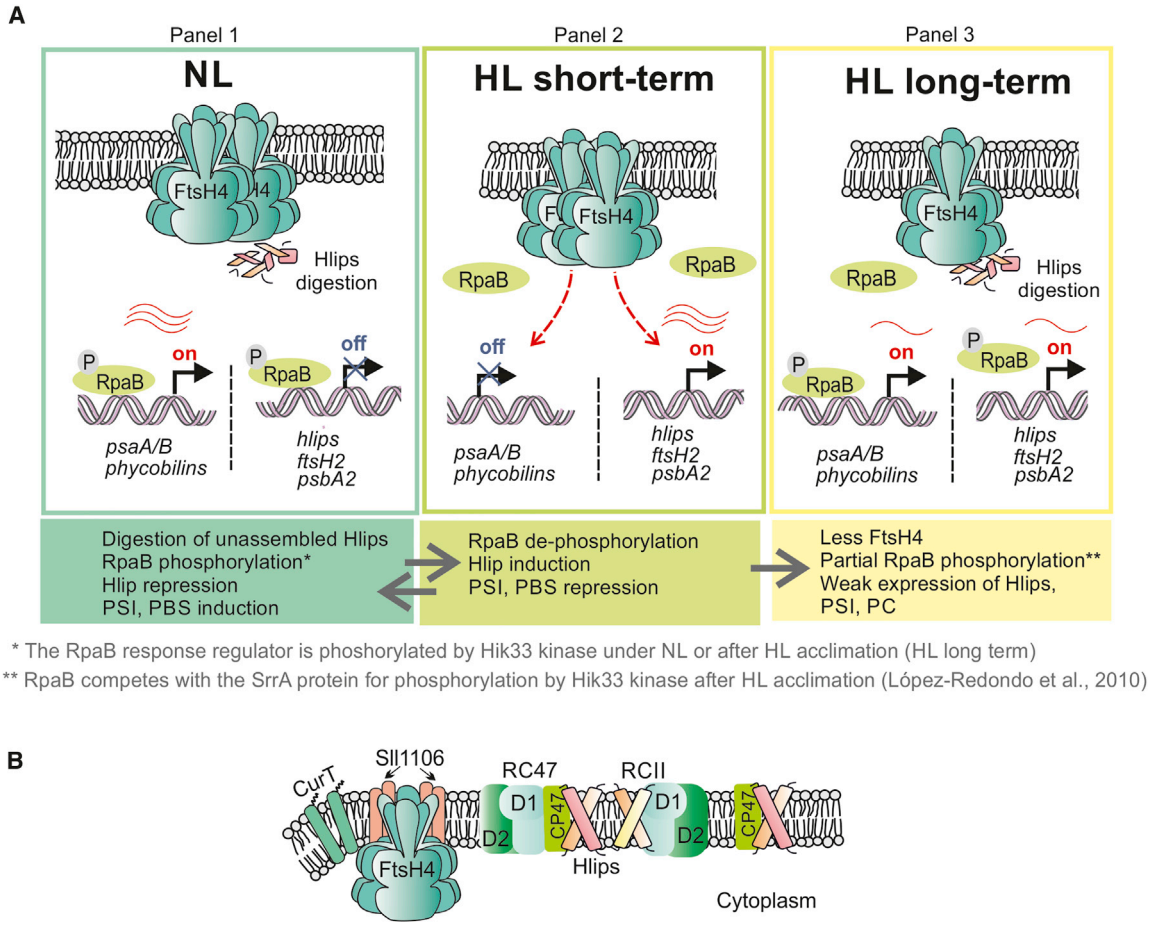

Figure 7. Model for FtsH4 role in acclimation to HL and its localization in the TM.

(A) The role of FtsH4 in the transcriptional and proteolytic regulation of Hlips under various light conditions. Under NL (panel 1), Hik33-phosphorylated RpaB represses expression of HL-inducible genes and activates expression of PSI and phycobiliprotein (PBS) genes. Unnecessary Hlips are degraded by FtsH4. After a shift to high light (HL; panel 2), Hik33 is transiently switched to the phosphatase conformation, leading to RpaB dephosphorylation and its release from DNA binding. This causes derepression of HL-inducible genes and repression of PSI/PBS genes. The presence of FtsH4 stimulates Hlip induction and at the same time PSI/PBS repression. FtsH4 might regulate the level of RpaB response regulator or possibly some σ factor from group 2, such as SigD (Sll2012) or SigE (Sll1689) (Srivastava et al., 2020). After long-term HL exposure (acclimation to HL, panel 3), Hik33 regains kinase activity but preferentially phosphorylates SrrA (a product of HL-inducible genes), and RpaB is only partially phosphorylated. Therefore, both Hlips and PSI/PBS are expressed, but weakly. Unnecessary Hlips are degraded by FtsH4. The red wavy lines represent mRNA, and their number indicates the amount of transcript.

(B) Co-localization of the FtsH4 protease with proteins connected to PSII assembly. Proteins co-purified with FtsH4 are assumed to directly interact or co-localize with the protease. These were Sll1106, CurT (Slr0483), and several subunits of PSII, preferentially CP47. FtsH4, together with Sll1106 and CurT, was also found to be associated with the D1/D2 assembly intermediates (Knoppová et al., 2022). RC47 and RCII: PSII intermediates lacking CP43 or both CP47 and CP43 core antennas, respectively.

membrane nanoscale regions. Their organization resembles "blobs" or occasionally "tunnels" that are slightly shifted outside and inside the TM in comparison with Chl autofluorescence of thylakoids (Figure 6) and strikingly resemble sub-cellular distributions of CurT protein, as observed by Heinz et al. (2016). It is important to note that FtsH4–GFP blobs have lower Chl or phycobilin fluorescence as deduced from detailed 2D SIM analysis. This shows that biogenesis centers are likely to be localized outside of the Chl/phycobilin-abundant microdomains (Strašková et al., 2019). These small cyanobacterial TM areas with such low Chl/phycobilin fluorescence were proposed to be a border between two dominant microdomains rich in PSI or PSII, respectively (Strašková et al., 2019). In higher plants, comparable boundaries between PSII- and PSI-rich zones occur at the grana margins. Interestingly, the grana margins also have been suggested as a region of high protein assembly activity connected with PSII repair and regulation of FtsH activity (Kato and Sakamoto, 2018). We hypothesize that special TM compartments where FtsH4 concentrates are identical or overlap with the compartment in which biogenesis of photosynthetic complexes takes place. There, FtsH4 supervises the assembly process by controlling the level of auxiliary proteins such as Hlips. When Hlips are released from the reaction center during PSII assembly, they are either bound to another intermediate or become available for FtsH4 digestion, thereby optimizing the assembly process.

METHODS

Construction and cultivation of *Synechocystis* strains

Synechocystis substrain GT-P (Tichý et al., 2016) was used as the WT in both phenotype analysis and genetic modifications. The FtsH4-less strain ΔFtsH4 was constructed by replacing the sequence between the SmaI sites of its gene *sll1463* (cyanobase designation) with a chloramphenicol resistance cassette (Supplemental Table 6, list of primers). The DNA construct was first cloned into the pGEM-T Easy vector and then used to transform WT *Synechocystis*. Strains expressing FtsH4 and Sll1106 with a C-terminally attached 3× FLAG-tag under the *psbA2* promotor were constructed as described in Skotnicová et al. (2018). The candidate gene was cloned into the pPD-CFLAG vector, which was used to transform the WT, and the resulting mutants were screened for kanamycin resistance. The A3 strain, which lacks *psbAI* and *psbAII* genes (Metz et al., 1989), was used as a control for the F4CF strains. The FtsH2-less versions of the ΔFtsH4 and F4CF mutants were prepared by transformation with genomic DNA from the ΔFtsH2 strain (Boehm et al., 2012), and the resulting double mutants were screened for chloramphenicol resistance.

The previously described FtsH4–GFP plasmid (Krynická et al., 2014) was used for preparation of His-tagged FtsH4 under the native promoter using SspDI and SphI restriction sites and removing the thrombin cleavage site, GFP, and a strep II tag from the plasmid. The 6xHis sequence was inserted at the C terminus using a reverse PCR primer (Supplemental Table 6, list of primers). The D515N mutation was inserted into the plasmid using a QuikChange II XL site-directed mutagenesis kit (Agilent Technologies). The resulting plasmids were transformed into *Synechocystis*, and transformants were fully segregated by an increasing concentration of antibiotics. The presence of the D515N mutation within His-tagged FtsH4 was confirmed by sequencing.

To obtain His-tagged HliD, we cloned the *hliD* gene into the pPD-NFLAG plasmid (Hollingshead et al., 2012) using NdeI and BglII restriction sites with removal of the FLAG-tag. The 8xHis sequence was inserted at the N terminus using a forward PCR primer (Supplemental Table 6, list of primers). The construct was transformed into Δ*hliD* (Chidgey et al., 2014). The previously constructed His-HliA/Δ*hliA*, His-HliB/Δ*hliB* (Konert et al., 2022), and His-HliC/Δ*hliC* (Shukla et al., 2018) strains were used for isolation of His-tagged Hlips for the FtsH4 proteolytic assay.

Liquid cultures were grown in BG-11 in Erlenmeyer flasks at 28°C on a rotary shaker (120 rpm), with mixotrophically grown cultures supplemented with 5 mM glucose. Illumination conditions were NL (40 μmol photons m^{-2} s^{-1}), HL (500 μmol photons m^{-2} s^{-1}), or LL (5 μmol photons m^{-2} s^{-1}). For the cold stress experiment, strains were cultivated at 18°C under 160 μmol photons m^{-2} s^{-1}. For SP experiments, liquid cultures in the exponential phase were diluted to OD_{750nm} = 0.1 and grown autotrophically without any other dilution for 14 days at NL. For inhibition of protein synthesis, liquid cultures were supplemented with LIN (100 μg ml^{-1} final concentration) and incubated at HL as specified in the results.

Synechocystis strains for purification were grown in 1-L cylinders bubbled with air at 100 μmol photons m^{-2} s^{-1} under white fluorescence tubes, and the light intensity was increased to 300 μmol photons m^{-2} s^{-1} for 16 h before harvesting.

Whole-cell absorption spectroscopy and Chl determination

Absorption spectra of whole cells, resuspended to constant OD_{750nm}, were acquired at room temperature using a UV-3000 spectrophotometer (Shimadzu, Japan). For routine Chl determination, methanol extracts of cell pellets or membranes were analyzed spectroscopically according to Porra et al. (1989).

Membrane isolation

Approximately 100 ml of cells at an OD_{750nm} of ∼0.8 was harvested by centrifugation at 6000 × *g* for 10 min and resuspended in buffer A for protein analysis and FLAG-tagged pulldown (25 mM MES [pH 6.5], 20 mM Ca^{2+}, 2 mM Mg^{2+}, 25% glycerol) or buffer B for His-tagged pulldown (25 mM Na phosphate buffer [pH 8], 50 mM NaCl, 10% glycerol). Cells were mixed with 100- to 200-μm-diameter glass beads in a 1:1 ratio (1 vol of dense cell solution with 1 vol of glass beads) and broken (6 × 20 s) using a mini-bead beater. To separate soluble and membrane fractions, we centrifuged samples at 30 000 × *g* for 20 min at 4°C. Pelleted membranes were washed once with an excess of buffer and then resuspended in 150 μl of buffer A/B.

Electrophoresis and immunoblotting

For 1D SDS–PAGE, membrane proteins were solubilized with 2% SDS (w/v) and 1% (w/v) dithiothreitol for 30 min at room temperature and analyzed by SDS–PAGE in a denaturing 12%–20% polyacrylamide gel containing 7 M urea or in 4%–15% TGX precast gels (Bio-Rad). For native electrophoresis, the proteins were separated on a 4%–14% (w/v) polyacrylamide CN–PAGE gel as described by Komenda et al. (2019) or a 4%–15% TGX precast gel (Bio-Rad). The protein gels were scanned, and the Chl fluorescence image was taken by a LAS-4000 camera (Fuji). Individual components of protein complexes were resolved by incubating the gel strip from the first dimension in 2% (w/v) SDS and 1% (w/v) dithiothreitol for 30 min at room temperature; then proteins were separated in the second dimension by a 12%–20% linear gradient SDS–PAGE gel containing 7 M urea. Proteins in gels were stained with SYPRO Orange (Sigma-Aldrich) or Coomassie blue (Bio-Rad).

For detection by a specific antibody, proteins were transferred from the SDS gel to a polyvinylidene fluoride membrane (Immobilon-P; Merck Millipore). The membrane was incubated with the primary antibody and subsequently with an anti-rabbit secondary antibody conjugated with horseradish peroxidase (Sigma-Aldrich). Chemiluminescence was imaged using the LAS-4000 camera.

The primary antibodies were specific for the following proteins used in this study: D1 (Komenda et al., 2005), D2 (Komenda et al., 2004), FtsH4 (Boehm et al., 2012), HliC (Konert et al., 2022), HliA/B (cat. no. AS10 1603; Agrisera), HliD (cat. no. AS10 1615; Agrisera), PetC (cat. no. AS08 330; Agrisera), PsaB (cat. no. AS10 695; Agrisera), and FLAG (Abgent). The Sll1106 antibody was created against the peptide RTSLSQDEESQLQ.

Purification of tagged proteins

For the purification of His-tagged FtsH4 variants, 3.5 L of cells was broken using glass beads as described above in buffer B with EDTA-free protease inhibitor (Sigma). The pelleted membrane fraction, prepared essentially as described in Koskela et al. (2020), was resuspended in buffer B (∼0.5 mg Chl/ml) and solubilized for 60 min at 10°C with 1% 4-trans-propylcyclohexyl α-maltoside (TPCC). Finally, insoluble contaminants were removed by centrifugation (47 000 × *g*, 20 min), and the concentration of NaCl in the supernatant was adjusted to 0.5 M. The supernatant was further supplemented with 10 mM imidazole and incubated with the resin for 60 min (1 ml Protino Ni–NTA agarose; Macherey-Nagel, Germany). Afterward, the supernatant was loaded on a chromatography column for washing steps. Proteins bound to the column were washed first with 20 ml of buffer B containing 0.5 M NaCl, 10 mM imidazole, and 0.04% TPCC, then 20 ml of buffer B containing 20 mM imidazole and 0.04% TPCC, and finally with 10 ml of 40 mM imidazole with 0.04% TPCC. Proteins were eluted using 6 ml of buffer B containing 200 mM imidazole, 0.04% TPCC, and 1.5 mM ATP. Proteins eluted from the Ni-NTA column were concentrated ∼12× on Amicon 100-kDa micro-concentrators (Millipore).

FLAG-tagged FtsH4 from F4CF and F4CF/ΔFtsH2 strains was purified in buffer A as described in Koskela et al. (2020) using 1% TPCC instead of β-DDM for membrane solubilization. In order to remove non-specific or transiently interacting proteins in F4CF/ΔFtsH2 membranes, 10 wash steps were used instead of 5.

FtsH *in vitro* assay

Hlips, Sll1106, and proteolytically active or inactive variants of FtsH4 were isolated from the *Synechocystis* membrane fraction as described above. The FtsH protease assay was carried out essentially according to Tomoyasu et al. (1995) and Srinivasan et al. (2008) using 0.3 μg of total FtsH4 eluate and 0.2 μg of the substrate eluate (Hlip or Sll1106). To inhibit activity of the active FtsH variant, the reaction was supplemented with cOmplete Protease Inhibitor Cocktail (Roche) containing EDTA. The reaction was carried out in 20 μl. Composition of the reaction buffer was 25 mM MES (pH 6.5), 5% glycerol, 2 mM Mg^{2+}, 2 mM Ca^{2+}, 0.4 μM Zn^{2+}, 3 mM ATP, and 0.04% TPCC. All samples were incubated for 3 h at 37°C. After incubation, the samples were denatured by 1% SDS and separated by 1D SDS–PAGE; the presence of Hlips and FtsH4 was detected by specific antibodies, and Sll1106 was detected by FLAG-specific antibody. For substrate quantification, the percentage of the substrate in a particular reaction sample relates to the initial substrate amount (100%); data are presented as means of three measurements of three independent reactions ± standard deviation. Quantification of bands was performed with ImageQuant TL software (GE Healthcare, Uppsala, Sweden).

Radiolabeling of proteins

Radioactive pulse (for 2D analysis) and pulse-chase (for 1D analysis) labeling of the cells was performed using a mixture of [^{35}S]Met and [^{35}S]Cys (Hartmann Analytic, Braunschweig, Germany) as described previously (Dobáková et al., 2009).

Proteomics

Protein bands were excised from the SDS–PAGE and CN–PAGE gels and digested with trypsin according to Pandey et al. (2000). The peptides extracted from the SDS–PAGE gel were analyzed by nano-flow liquid chromatography (nanoLC) coupled to an Amazon ion-trap mass spectrometer (Bruker) according to Mothersole et al. (2016), except that peptide separation was achieved using a 20-min gradient. Spectra were converted to MGF format using a script provided in DataAnalysis v.4.1 software (Bruker Daltonics) and then submitted for searching using Byonic v.2.9.38 (Protein Metrics) against the *Synechocystis* sp. PCC 6803 reference proteome database downloaded on 14 May 2021 (https://www.uniprot.org/proteomes/UP000001425). Search parameters were as per default for trypsin except that carbamidomethylation was selected as a fixed modification for Cys and oxidation (variable, common, maximum of two per peptide) for Met. Both precursor and fragment mass tolerances were set at 0.5 Da, fragmentation type was CID low energy, and precursor and charge assignments were set as originally assigned. Peptides derived from the protein complexes resolved by CN–PAGE were analyzed by nanoLC coupled to a Q Exactive HF mass spectrometer (Thermo Fisher Scientific) according to Flannery et al. (2021), except that a 75-min gradient was used for peptide separation. Mass spectra were submitted for database searching with fixed and variable modifications as above but without prior format conversion. All other parameters, including mass tolerances, were as per default.

WT TMs (100 μg protein, Bio-Rad DC assay) were solubilized in 2% (w/v) SDS and 60 mM dithiothreitol with brief vortexing at room temperature. Eluates from FLAG pulldown preparations were diluted with 100 mM triethylammonium bicarbonate (pH 8.5; Sigma-Aldrich) to reduce the TPCC concentration to below its CMC at 0.036 mM, then concentrated to <100 μL using an Amicon 10-kDa centrifugal ultrafilter. Proteins from membranes and FLAG eluates were precipitated using a 2D clean-up kit (Cytiva) according to the manufacturer's protocol and then processed for nanoLC-MS analysis according to Hitchcock et al. (2016). Mass spectra were acquired using 180-min (membranes) and 75-min (FLAG eluates) nanoLC gradients online to a Q Exactive HF instrument, with database searching performed as above.

Selected proteins were quantified by the iBAQ method (Schwanhäusser et al., 2011), with abundance scores derived by normalizing the total ion intensity (in the case of WT membranes and F4CF/ΔFtsH2 FLAG eluate) or mean ion intensity (in the case of F4CF and WT FLAG-eluates) displayed in the Byonic database search results to the number of theoretical tryptic peptides with 6–30 residues.

The MS proteomics data have been deposited to the ProteomeXchange Consortium via the PRIDE partner repository with the dataset identifier PXD033240.

Confocal microscopy

Images of *Synechocystis* cells immobilized on an agar plate were acquired using a laser scanning confocal microscope (Zeiss LSM 880; Carl Zeiss Microscopy, Germany) equipped with a plan-apochromatic 63×/1.4 oil DIC M27 objective lens. The three-channel pictures were obtained by two sequential images with different parameters. PBS emission was excited by a 633-nm laser (dichroic mirror: MBS 488/543/633) and detected at 642–677 nm. In the following sequence, the Chl autofluorescence from PSII and GFP fluorescence from FtsH4–GFP were both excited with a 488-nm Ar laser (dichroic mirror: MBS 488) and detected at 696–758 and 491–544 nm, respectively, with 8-bit, 512 × 512 pixel image acquisition. 3D images were obtained from z stack scans of 150-nm steps. The raw z stack images were processed by ZEN Black software (Carl Zeiss Microscopy, Germany).

SIM

Synechocystis cells were fixed with 4% formaldehyde solution at 37°C for 10 min, then attached to poly-L-lysine-coated coverslips and mounted in VECTASHIELD antifade medium (Vector Laboratories). SIM was performed on a DeltaVision OMX V4 microscope (GE Healthcare) equipped with a Blaze-3D SIM module for introducing patterned illumination to the sample plane and a 60× 1.42 NA oil plan-apochromatic objective lens. Chl and GFP fluorescence images were collected through 683/40 nm and 528/48 bandpass filters, respectively. The patterned illumination was projected through five separate phases for each of three different, equally spaced angles, yielding 15 images per 2D image. 3D images were acquired via 2D sectioning with a separation of 125 nm. The final deconvoluted super-resolution image was reconstructed with softWoRx OMX 6.0 software (GE Healthcare). For processing, images were thresholded and converted to 16-bit with the SIMcheck plugin for ImageJ (Ball et al., 2015). Radial profiles were generated via custom MATLAB code (MathWorks) that sweeps 360° around the cell and generates a mean intensity profile. 3D renders were generated with Imaris (Oxford Instruments). To quantify the variation in membrane clustering across the four conditions, we performed the following: the means and standard deviations of pixel-based segments of TMs were found in FIJI. The standard deviations were then normalized to the mean fluorescence intensity and then log-transformed to take into account ratiometric skewing. A one-way ANOVA was then performed, followed by multiple comparison correction with Tukey's Honestly Significant Difference procedure to calculate *P* values (Supplemental Figure 11).

SUPPLEMENTAL INFORMATION

Supplemental information is available at *Plant Communications Online*.

FUNDING

This work was supported by the Grant Agency of the Czech Republic (19-08900Y to V.K.; 22-03092S to A.W.). M.J.D. acknowledges support from the Biotechnology and Biological Sciences Research Council (UK) (BB/M012166/1). J.K., P.J.J., and C.N.H. gratefully acknowledge financial support from the European Research Council, Synergy award 854126. C.N.H. and P.J.J. were also supported by award BB/M000265/1 from the Biotechnology and Biological Sciences Research Council (BBSRC UK).

AUTHOR CONTRIBUTIONS

V.K. performed most experiments, including the protease assay of FtsH4; P.S., V.K., and A.W. performed purification of tagged proteins; P.J.J.

performed MS measurement and analyses; J.Y. and P.S. constructed the new strains used in this work; S.B. performed SIM measurement and analyses; P.S. and R.K. performed confocal microscopy measurement; V.K. made spectroscopic measurements and electrophoretic analyses; J.K. performed radioactive labeling of proteins; C.N.H. and M.J.D. were involved in experimental design; V.K., J.K., P.S., P.J.J., and P.J.N. wrote the article; J.K., V.K., C.N.H., P.J.N., and M.J.D. acquired the funding; V.K. supervised the project; all authors discussed the results and commented on the article.

ACKNOWLEDGMENTS

No conflict of interest is declared.

Received: June 20, 2022
Revised: November 11, 2022
Accepted: November 29, 2022
Published: December 5, 2022

REFERENCES

Allen, D.J., and Ort, D.R. (2001). Impacts of chilling temperatures on photosynthesis in warm-climate plants. Trends Plant Sci. **6**:36–42. https://doi.org/10.1016/s1360-1385(00)01808-2.

Ball, G., Demmerle, J., Kaufmann, R., Davis, I., Dobbie, I.M., and Schermelleh, L. (2015). SIMcheck: a toolbox for successful super-resolution structured illumination microscopy. Sci. Rep. **5**:15915. https://doi.org/10.1038/srep15915.

Biswal, B., Joshi, P.N., Raval, M.K., and Biswal, U.C. (2011). Photosynthesis, a global sensor of environmental stress in green plants: stress signalling and adaptation. Curr. Sci. **101**:47–56.

Boehm, M., Yu, J., Krynická, V., Barker, M., Tichý, M., Komenda, J., Nixon, P.J., and Nield, J. (2012). Subunit organization of a *Synechocystis* hetero-oligomeric thylakoid FtsH complex involved in photosystem II repair. Plant Cell **24**:3669–3683. https://doi.org/10.1105/tpc.112.100891.

Casella, S., Huang, F., Mason, D., Zhao, G.Y., Johnson, G.N., Mullineaux, C.W., and Liu, L.N. (2017). Dissecting the native architecture and dynamics of cyanobacterial photosynthetic machinery. Mol. Plant **10**:1434–1448. https://doi.org/10.1016/j.molp.2017.09.019.

Dobáková, M., Sobotka, R., Tichý, M., and Komenda, J. (2009). Psb28 protein is involved in the biogenesis of the photosystem II inner antenna CP47 (PsbB) in the cyanobacterium *Synechocystis* sp PCC 6803. Plant Physiol. **149**:1076–1086. https://doi.org/10.1104/pp.108.130039.

Ferro, M., Brugière, S., Salvi, D., Seigneurin-Berny, D., Court, M., Moyet, L., Ramus, C., Miras, S., Mellal, M., Le Gall, S., et al. (2010). AT_CHLORO, a comprehensive chloroplast proteome database with subplastidial localization and curated information on envelope proteins. Mol. Cell. Proteomics **9**:1063–1084. https://doi.org/10.1074/mcp.M900325-MCP200.

Flannery, S.E., Hepworth, C., Wood, W.H.J., Pastorelli, F., Hunter, C.N., Dickman, M.J., Jackson, P.J., and Johnson, M.P. (2021). Developmental acclimation of the thylakoid proteome to light intensity in *Arabidopsis*. Plant J. **105**:223–244. https://doi.org/10.1111/tpj.15053.

Funk, C., and Vermaas, W. (1999). A cyanobacterial gene family coding for single-helix proteins resembling part of the light-harvesting proteins from higher plants. Biochemistry **38**:9397–9404. https://doi.org/10.1021/bi990545+.

Heinz, S., Rast, A., Shao, L., Gutu, A., Gügel, I.L., Heyno, E., Labs, M., Rengstl, B., Viola, S., Nowaczyk, M.M., et al. (2016). Thylakoid membrane architecture in *Synechocystis* depends on CurT, a homolog of the granal CURVATURE THYLAKOID1 proteins. Plant Cell **28**:2238–2260. https://doi.org/10.1105/tpc.16.00491.

Hitchcock, A., Jackson, P.J., Chidgey, J.W., Dickman, M.J., Hunter, C.N., and Canniffe, D.P. (2016). Biosynthesis of chlorophyll a in a purple bacterial phototroph and assembly into a plant chlorophyll-protein complex. ACS Synth. Biol. **5**:948–954. https://doi.org/10.1021/acssynbio.6b00069.

Hollingshead, S., Kopecná, J., Jackson, P.J., Canniffe, D.P., Davison, P.A., Dickman, M.J., Sobotka, R., and Hunter, C.N. (2012). Conserved chloroplast open-reading frame ycf54 is required for activity of the magnesium protoporphyrin monomethylester oxidative cyclase in *Synechocystis* PCC 6803. J. Biol. Chem. **287**:27823–27833. https://doi.org/10.1074/jbc.M112.352526.

Chidgey, J.W., Linhartová, M., Komenda, J., Jackson, P.J., Dickman, M.J., Canniffe, D.P., Koník, P., Pilný, J., Hunter, C.N., and Sobotka, R. (2014). A Cyanobacterial chlorophyll synthase-HliD complex associates with the Ycf39 protein and the YidC/Alb3 insertase. Plant Cell **26**:1267–1279. https://doi.org/10.1105/tpc.114.124495.

1. **Ito, K., and Akiyama, Y.** (2005). Cellular functions, mechanism of action, and regulation of FtsH protease. Annu Rev Microbiol **59**:211–231. https://doi.org/10.1146/annurev.micro.59.030804.121316.

Järvi, S., Suorsa, M., Tadini, L., Ivanauskaite, A., Rantala, S., Allahverdiyeva, Y., Leister, D., and Aro, E.M. (2016). Thylakoid-bound FtsH proteins facilitate proper biosynthesis of photosystem I. Plant Physiol. **171**:1333–1343. https://doi.org/10.1104/pp.16.00200.

Kato, Y., and Sakamoto, W. (2018). FtsH protease in the thylakoid membrane: physiological functions and the regulation of protease activity. Front. Plant Sci. **9**:855. https://doi.org/10.3389/fpls.2018.00855.

Kato, Y., Miura, E., Matsushima, R., and Sakamoto, W. (2007). White leaf sectors in yellow variegated2 are formed by viable cells with undifferentiated plastids. Plant Physiol. **144**:952–960. https://doi.org/10.1104/pp.107.099002.

Knoppová, J., Sobotka, R., Tichy, M., Yu, J., Koník, P., Halada, P., Nixon, P.J., and Komenda, J. (2014). Discovery of a chlorophyll binding protein complex involved in the early steps of photosystem II sssembly in *Synechocystis*. Plant Cell **26**:1200–1212. https://doi.org/10.1105/tpc.114.123919.

Knoppová, J., Sobotka, R., Yu, J., Bečková, M., Pilný, J., Trinugroho, J.P., Csefalvay, L., Bína, D., Nixon, P.J., and Komenda, J. (2022). Assembly of D1/D2 complexes of photosystem II: binding of pigments and a network of auxiliary proteins. Plant Physiol. **189**:790–804. https://doi.org/10.1093/plphys/kiac045.

Komenda, J., and Sobotka, R. (2016). Cyanobacterial high-light-inducible proteins - protectors of chlorophyll-protein synthesis and assembly. Biochim. Biophys. Acta **1857**:288–295. https://doi.org/10.1016/j.bbabio.2015.08.011.

Komenda, J., Tichý, M., and Eichacker, L.A. (2005). The PsbH protein is associated with the inner antenna CP47 and facilitates D1 processing and incorporation into PSII in the cyanobacterium *Synechocystis* PCC 6803. Plant Cell Physiol. **46**:1477–1483. https://doi.org/10.1093/pcp/pci159.

Komenda, J., Sobotka, R., and Nixon, P.J. (2012). Assembling and maintaining the Photosystem II complex in chloroplasts and cyanobacteria. Curr. Opin. Plant Biol. **15**:245–251. https://doi.org/10.1016/j.pbi.2012.01.017.

Komenda, J., Krynická, V., and Zakar, T. (2019). Isolation of thylakoid membranes from the cyanobacterium *Synechocystis* sp. PCC 6803 and analysis of their photosynthetic pigment-protein complexes by Clear Native-PAGE. Bio-Protocol **9**:e3126. https://doi.org/10.21769/BioProtoc.3126.

Komenda, J., Reisinger, V., Müller, B.C., Dobáková, M., Granvogl, B., and Eichacker, L.A. (2004). Accumulation of the D2 protein is a key regulatory step for assembly of the photosystem II reaction center

complex in *Synechocystis* PCC 6803. J. Biol. Chem. **279**:48620–48629. https://doi.org/10.1074/jbc.M405725200.

Komenda, J., Barker, M., Kuviková, S., de Vries, R., Mullineaux, C.W., Tichý, M., and Nixon, P.J. (2006). The FtsH protease *slr0228* is important for quality control of photosystem II in the thylakoid membrane of *Synechocystis* sp PCC 6803. J. Biol. Chem. **281**:1145–1151. https://doi.org/10.1074/jbc.M503852200.

Konert, M.M., Wysocka, A., Koník, P., and Sobotka, R. (2022). High-light-inducible proteins HliA and HliB: pigment binding and protein-protein interactions. Photosynth. Res. **152**:317–332. https://doi.org/10.1007/s11120-022-00904-z.

Kopecná, J., Komenda, J., Bucinská, L., and Sobotka, R. (2012). Long-term acclimation of the cyanobacterium *Synechocystis* sp PCC 6803 to high light is accompanied by an enhanced production of chlorophyll that is preferentially channeled to trimeric photosystem I. Plant Physiol. **160**:2239–2250. https://doi.org/10.1104/pp.112.207274.

Kopf, M., Klähn, S., Scholz, I., Matthiessen, J.K.F., Hess, W.R., and Voß, B. (2014). Comparative analysis of the primary transcriptome of *Synechocystis* sp PCC 6803. DNA Res. **21**:527–539. https://doi.org/10.1093/dnares/dsu018.

Koskela, M.M., Skotnicová, P., Kiss, É., and Sobotka, R. (2020). Purification of protein-complexes from the cyanobacterium *Synechocystis* sp. PCC 6803 using FLAG-affinity chromatography. Bio. Protoc. **10**:e3616. https://doi.org/10.21769/BioProtoc.3616.

Krynická, V., Shao, S., Nixon, P.J., and Komenda, J. (2015). Accessibility controls selective degradation of photosystem II subunits by FtsH protease. Nat. Plants **1**:15168. https://doi.org/10.1038/nplants.2015.168.

Krynická, V., Tichý, M., Krafl, J., Yu, J., Kaňa, R., Boehm, M., Nixon, P.J., and Komenda, J. (2014). Two essential FtsH proteases control the level of the Fur repressor during iron deficiency in the cyanobacterium *Synechocystis* sp PCC 6803. Mol. Microbiol. **94**:609–624. https://doi.org/10.1111/mmi.12782.

Krynická, V., Georg, J., Jackson, P.J., Dickman, M.J., Hunter, C.N., Futschik, M.E., Hess, W.R., and Komenda, J. (2019). Depletion of the FtsH1/3 proteolytic complex suppresses the nutrient stress response in the cyanobacterium *Synechocystis* sp strain PCC 6803. Plant Cell **31**:2912–2928. https://doi.org/10.1105/tpc.19.00411.

López-Redondo, M.L., Moronta, F., Salinas, P., Espinosa, J., Cantos, R., Dixon, R., Marina, A., and Contreras, A. (2010). Environmental control of phosphorylation pathways in a branched two-component system. Mol. Microbiol. **78**:475–489. https://doi.org/10.1111/j.1365-2958.2010.07348.x.

Los, D.A., Zorina, A., Sinetova, M., Kryazhov, S., Mironov, K., and Zinchenko, V.V. (2010). Stress sensors and signal transducers in cyanobacteria. Sensors **10**:2386–2415. https://doi.org/10.3390/s100302386.

Mann, N.H., Novac, N., Mullineaux, C.W., Newman, J., Bailey, S., and Robinson, C. (2000). Involvement of an FtsH homologue in the assembly of functional photosystem I in the cyanobacterium *Synechocystis* sp PCC 6803. FEBS Lett. **479**:72–77. https://doi.org/10.1016/s0014-5793(00)01871-8.

Metz, J.G., Nixon, P.J., Rögner, M., Brudvig, G.W., and Diner, B.A. (1989). Directed alteration of the D1 polypeptide of photosystem II: evidence that tyrosine-161 is the redox component, Z, connecting the oxygen-evolving complex to the primary electron donor, P680. Biochemistry **28**:6960–6969. https://doi.org/10.1021/bi00443a028.

Mothersole, D.J., Jackson, P.J., Vasilev, C., Tucker, J.D., Brindley, A.A., Dickman, M.J., and Hunter, C.N. (2016). PucC and LhaA direct efficient assembly of the light-harvesting complexes in *Rhodobacter sphaeroides*. Mol. Microbiol. **99**:307–327. https://doi.org/10.1111/mmi.13235.

Nishimura, K., Kato, Y., and Sakamoto, W. (2016). Chloroplast proteases: updates on proteolysis within and across suborganellar compartments. Plant Physiol. **171**:2280–2293. https://doi.org/10.1104/pp.16.00330.

Pandey, A., Andersen, J.S., and Mann, M. (2000). Use of mass spectrometry to study signaling pathways. Sci. STKE **2000**:pl1. https://doi.org/10.1126/stke.2000.37.pl1.

Porra, R.J., Thompson, W.A., and Kriedemann, P.E. (1989). Determination of accurate extinction coefficients and simultaneous equations for assaying chlorophylls a and b extracted with four different solvents: verification of the concentration of chlorophyll standards by atomic absorption spectroscopy. Biochim. Biophys. Acta Bioenerg. **975**:384–394. https://doi.org/10.1016/S0005-2728(89)80347-0.

Rachedi, R., Foglino, M., and Latifi, A. (2020). Stress signaling in cyanobacteria: a mechanistic overview. Life **10**:312.

Rast, A., Schaffer, M., Albert, S., Wan, W., Pfeffer, S., Beck, F., Plitzko, J.M., Nickelsen, J., and Engel, B.D. (2019). Biogenic regions of cyanobacterial thylakoids form contact sites with the plasma membrane. Nat. Plants **5**:436–446. https://doi.org/10.1038/s41477-019-0399-7.

Riediger, M., Hihara, Y., and Hess, W.R. (2018). From cyanobacteria and algae to land plants: the RpaB/Ycf27 regulatory network in transition. Perspectives in Phycology **5**:13–25. https://doi.org/10.1127/pip/2018/0078.

Riediger, M., Kadowaki, T., Nagayama, R., Georg, J., Hihara, Y., and Hess, W.R. (2019). Biocomputational analyses and experimental validation identify the regulon controlled by the redox-responsive transcription factor RpaB. iScience **15**:316–331. https://doi.org/10.1016/j.isci.2019.04.033.

Sacharz, J., Bryan, S.J., Yu, J., Burroughs, N.J., Spence, E.M., Nixon, P.J., and Mullineaux, C.W. (2015). Sub-cellular location of FtsH proteases in the cyanobacterium *Synechocystis* sp PCC 6803 suggests localised PSII repair zones in the thylakoid membranes. Mol. Microbiol. **96**:448–462. https://doi.org/10.1111/mmi.12940.

Sakayori, T., Shiraiwa, Y., and Suzuki, I. (2009). A *Synechocystis* homolog of SipA protein, Ssl3451, enhances the activity of the histidine kinase Hik33. Plant Cell Physiol. **50**:1439–1448. https://doi.org/10.1093/pcp/pcp089.

Shao, S., Cardona, T., and Nixon, P.J. (2018). Early emergence of the FtsH proteases involved in photosystem II repair. Photosynthetica **56**:163–177. https://doi.org/10.1007/s11099-018-0769-9.

Shukla, M.K., Llansola-Portoles, M.J., Tichý, M., Pascal, A.A., Robert, B., and Sobotka, R. (2018). Binding of pigments to the cyanobacterial high-light-inducible protein HliC. Photosynth. Res. **137**:29–39. https://doi.org/10.1007/s11120-017-0475-7.

Schwanhäusser, B., Busse, D., Li, N., Dittmar, G., Schuchhardt, J., Wolf, J., Chen, W., and Selbach, M. (2011). Global quantification of mammalian gene expression control. Nature **473**:337–342. https://doi.org/10.1038/nature10098.

Skotnicová, P., Sobotka, R., Shepherd, M., Hájek, J., Hrouzek, P., and Tichý, M. (2018). The cyanobacterial protoporphyrinogen oxidase HemJ is a new b-type heme protein functionally coupled with coproporphyrinogen III oxidase. J. Biol. Chem. **293**:12394–12404. https://doi.org/10.1074/jbc.RA118.003441.

Srinivasan, R., Rajeswari, H., and Ajitkumar, P. (2008). Analysis of degradation of bacterial cell division protein FtsZ by the ATP-dependent zinc-metalloprotease FtsH in vitro. Microbiol. Res. **163**:21–30. https://doi.org/10.1016/j.micres.2006.03.001.

Srivastava, A., Summers, M.L., and Sobotka, R. (2020). Cyanobacterial sigma factors: current and future applications for biotechnological

advances. Biotechnol. Adv. **40**:107517. https://doi.org/10.1016/j.biotechadv.2020.107517.

Stengel, A., Gügel, I.L., Hilger, D., Rengstl, B., Jung, H., and Nickelsen, J. (2012). Initial steps of photosystem II de novo asembly and preloading with manganese take place in biogenesis centers in. Plant Cell **24**:660–675. https://doi.org/10.1105/tpc.111.093914.

Strašková, A., Steinbach, G., Konert, G., Kotabová, E., Komenda, J., Tichý, M., and Kaňa, R. (2019). Pigment-protein complexes are organized into stable microdomains in cyanobacterial thylakoids. Biochim. Biophys. Acta Bioenerg. **1860**:148053. https://doi.org/10.1016/j.bbabio.2019.07.008.

Tichý, M., Bečková, M., Kopečná, J., Noda, J., Sobotka, R., and Komenda, J. (2016). Strain of *Synechocystis* PCC 6803 with aberrant assembly of photosystem II contains tandem duplication of a large chromosomal region. Front. Plant Sci. **7**:648. https://doi.org/10.3389/fpls.2016.00648.

Tomoyasu, T., Gamer, J., Bukau, B., Kanemori, M., Mori, H., Rutman, A.J., Oppenheim, A.B., Yura, T., Yamanaka, K., Niki, H., et al. (1995). *Escherichia coli* FtsH is a membrane-bound, ATP-dependent protease which degrades the heat-shock transcription factor sigma 32. EMBO J. **14**:2551–2560.

van Waasbergen, L.G., Dolganov, N., and Grossman, A.R. (2002). *nblS*, a gene involved in controlling photosynthesis-related gene expression during high light and nutrient stress in *Synechococcus elongatus* PCC 7942. J. Bacteriol. **184**:2481–2490. https://doi.org/10.1128/jb.184.9.2481-2490.2002.

Yao, D., Kieselbach, T., Komenda, J., Promnares, K., Prieto, M.A.H., Tichy, M., Vermaas, W., and Funk, C. (2007). Localization of the small CAB-like proteins in photosystem II. J. Biol. Chem. **282**:267–276. https://doi.org/10.1074/jbc.M605463200.

Yasuda, A., Inami, D., and Hanaoka, M. (2020). RpaB, an essential response regulator for high-light stress, is extensively involved in transcriptional regulation under light-intensity upshift conditions in *Synechococcus elongatus* PCC 7942. J. Gen. Appl. Microbiol. **66**:73–79. https://doi.org/10.2323/jgam.2020.01.010.

Yi, L., Liu, B., Nixon, P.J., Yu, J., and Chen, F. (2022). Recent advances in understanding the structural and functional evolution of FtsH proteases. Front. Plant Sci. **13**:837528.

Plant Communications, Volume *4*

Supplemental information

FtsH4 protease controls biogenesis of the PSII complex by dual regulation of high light-inducible proteins

Vendula Krynická, Petra Skotnicová, Philip J. Jackson, Samuel Barnett, Jianfeng Yu, Anna Wysocka, Radek Kaňa, Mark J. Dickman, Peter J. Nixon, C. Neil Hunter, and Josef Komenda

Supplementary Information

Supplementary Figures:

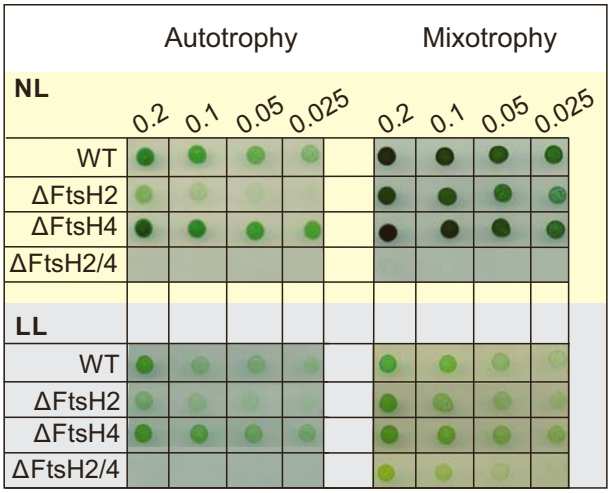

Supplementary Figure S1. Growth assay of WT, ΔFtsH2, ΔFtsH4, and ΔFtsH2/4 strains. Cells grown to exponential phase in liquid medium at normal light (NL, 40 µmol photons m^{-2} s^{-1}) were diluted to OD_{750nm} of 0.2, 0.1, 0.05, and 0.025, transferred on agar plates and exposed to NL or low light (LL, 5 µmol of photons m^{-2} s^{-1}) under autotrophic or mixotrophic conditions (5mM glucose supplement).

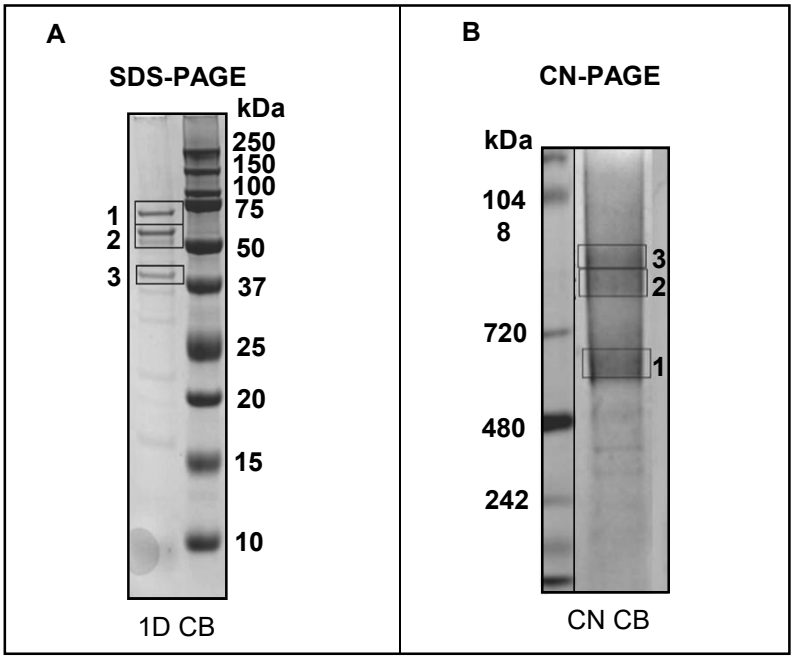

Supplementary Figure S2. In gel MS protein analysis of the F4CF/ΔFtsH2 pulldown. Pulldowns of FLAG-tagged FtsH4 isolated from the strain additionally lacking FtsH2 (F4CF/ΔFtsH2) were analyzed by 1D SDS-PAGE **(A)** or CN-PAGE **(B)**. Gels were stained by Coomassie Blue (CB). Protein bands in rectangles were cut out and analyzed by MS (MS results of SDS-PAGE or CN-PAGE are presented in Supplementary Table 2, 3 and Supplementary Dataset 2, respectively).

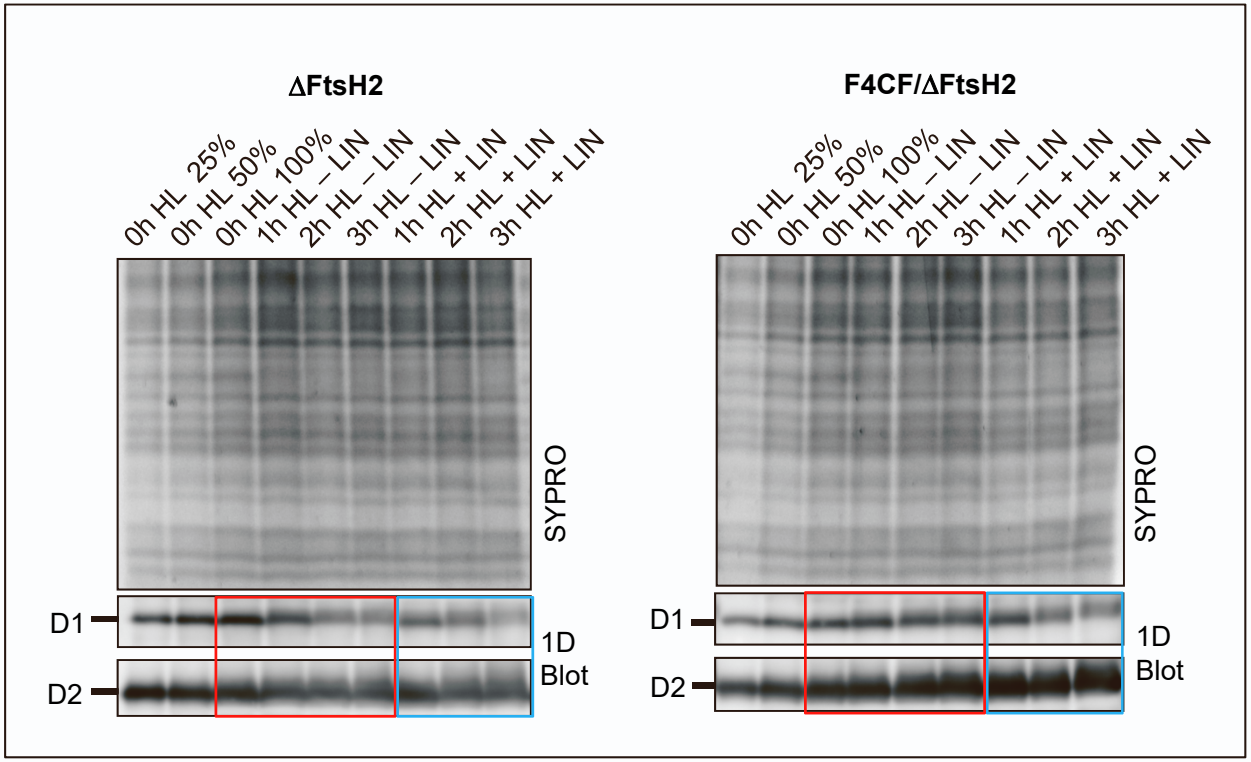

Supplementary Figure S3. The degradation of D1 and D2 proteins of photosystem II in the FtsH2-less (ΔFtsH2) and FtsH2-less strain overexpressing FLAG-tagged FtsH4 (F4CF/ΔFtsH2) under HL conditions. Cells were exposed to HL (500 µmol of photons m^{-2} s^{-1}) in the presence or absence of lincomycin (+LIN or –LIN, respectively) and their D1 and D2 protein content was assessed by immunoblotting using specific antibodies. Each sample contained 2 µg of Chl which corresponds to 100% in the dilution line. SYPRO Orange stained gel (SYPRO) is shown to document the equal loading.

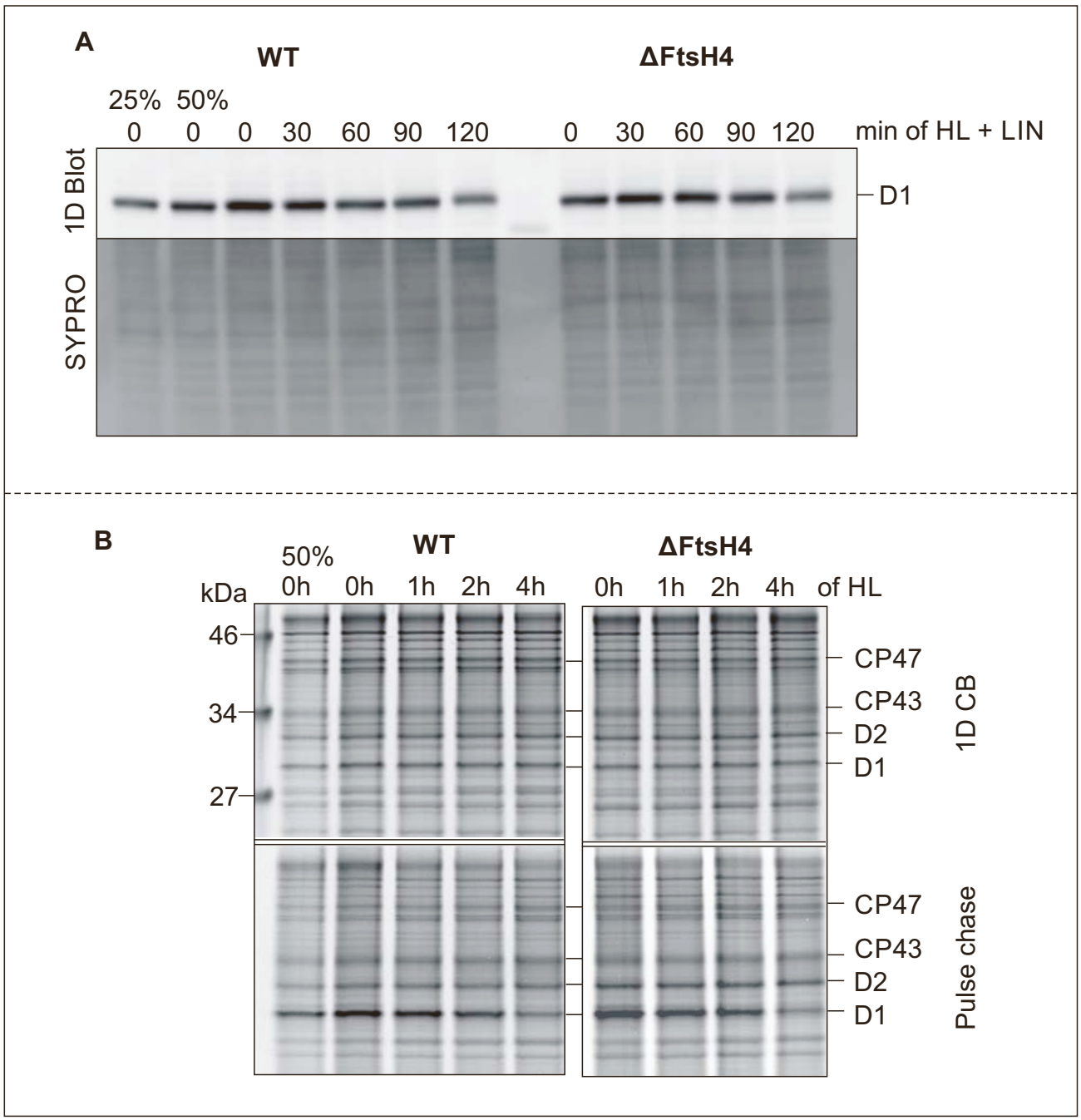

Supplementary Figure S4. Degradation of the D1 protein in WT and FtsH4-less strain (ΔFtsH4) under HL. A: Cells were exposed to HL (500 µmol of photons m^{-2} s^{-1}) in the presence of lincomycin (LIN) to prevent protein synthesis. Cell membranes were analyzed after 30, 60, 90, and 120 min of HL by immunoblotting using a specific antibody against D1. SYPRO Orange stained gel (SYPRO) is presented as a loading control. **B:** Degradation of D1 in HL monitored by radioactive pulse-chase labeling. Cells of both strains were subjected to 250 µmol of photons m^{-2} s^{-1} for 20 min in the presence of ^{35}[S] Met/Cys (0h). Then the cells were washed, supplemented with unlabeled Met/Cys, and subjected to HL. Membranes isolated from the labeled cells were analyzed by 1D SDS-PAGE. Each sample contained 2 µg of Chl which corresponds to 100% in the dilution line. The gel was stained with Coomassie Blue (CB) and, after drying, exposed in a phosphoimager overnight (Pulse chase).

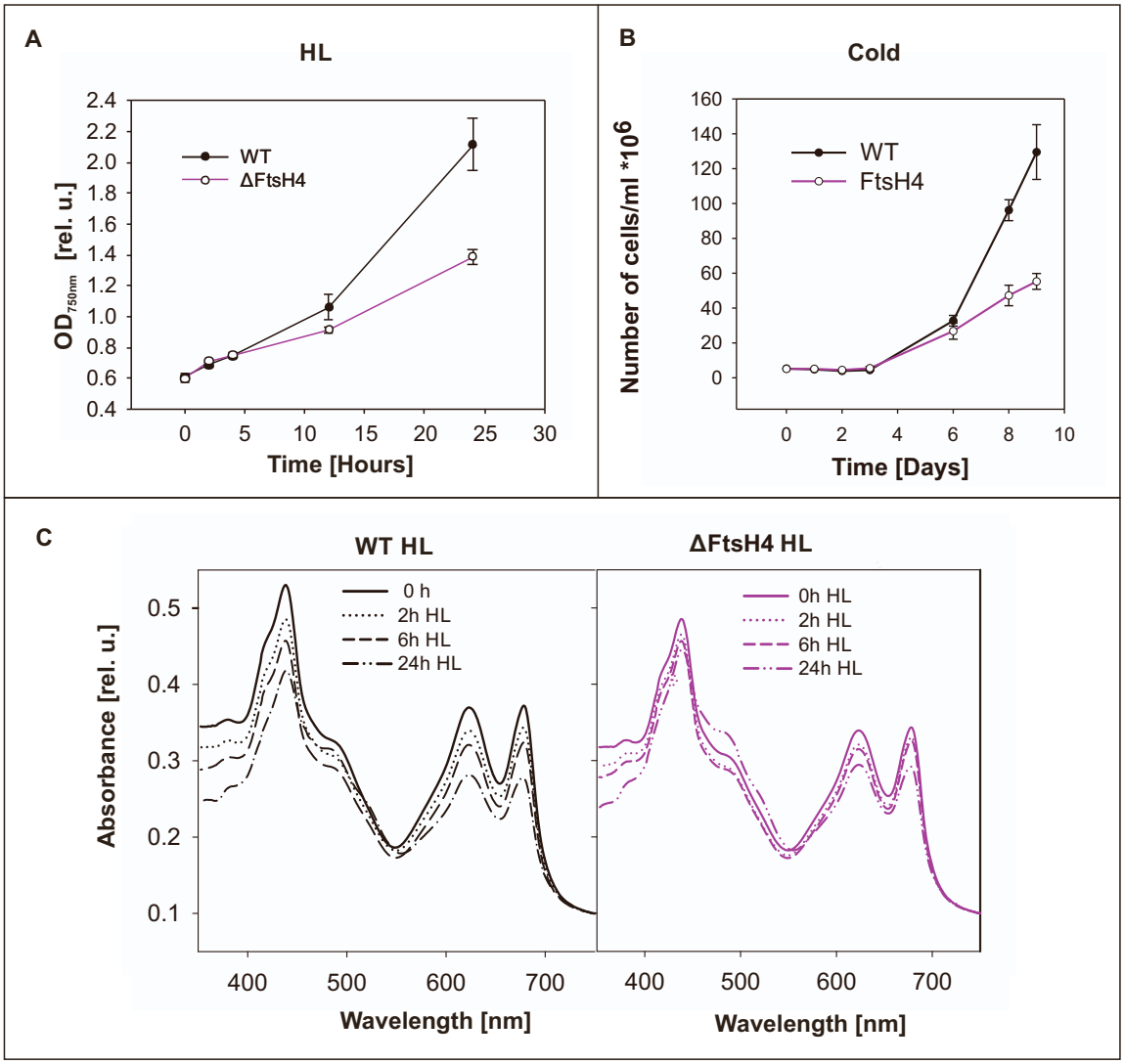

Supplementary Figure S5: Phenotype of WT and ΔFtsH4 under HL and cold stress conditions. A and B: Growth of WT and ΔFtsH4 cells during 24 h of the HL exposure (500 µmol of photons m^{-2} s^{-1}/28°C) monitored by OD_{750nm} measurement (A); and 9 days of cold stress (160 µmol of photons m^{-2} s^{-1}/18°C) monitored by cell counting using Multisizer 4, aperture 20 µm (B). Before the stress, cells were grown to exponential phase at normal light (40 µmol of photons m^{-2} s^{-1}/28°C) then diluted to OD_{750nm} 0.5 and exposed to the stress. Values are means of three biological replicates ± SD. **C**: Whole-cell absorption spectra of WT and ΔFtsH4 after 0, 2, 6, and 24 h of HL exposure.

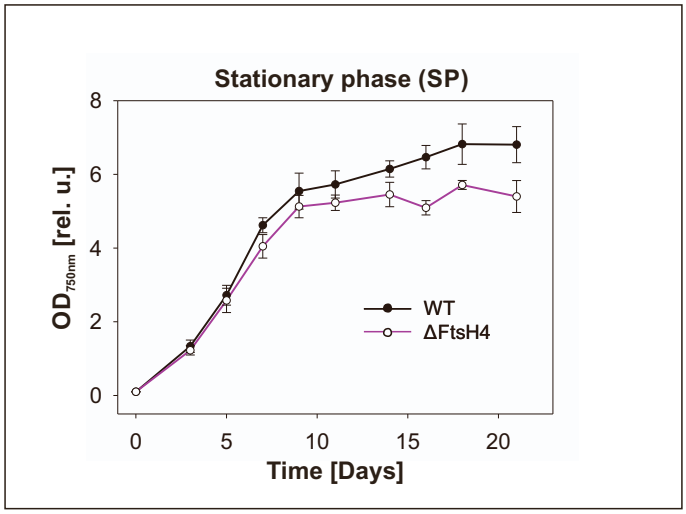

Supplementary Figure S6: Growth of WT and ΔFtsH4 until the stationary phase. WT and ΔFtsH4 cells in the exponential phase were diluted to OD_{750nm} 0.1 and grown without any other dilution for 21 days at NL. Both WT and ΔFtsH4 cells reached the stationary phase approximately on the 9th day. The final OD_{750nm} of the WT and ΔFtsH4 culture on 21st day of the growth was 6.8 or 5.4, respectively. Values are means of the four biological replicates ± SD.

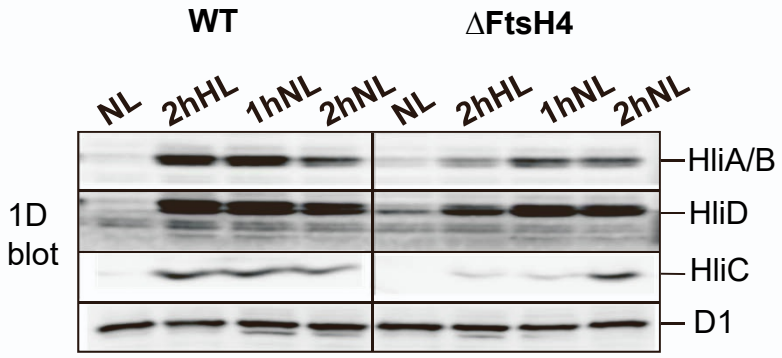

Supplementary Figure S7. Effect of *ftsH4* deletion on induction and accumulation of Hlips. Cells in exponential phase were grown at normal light (NL, 40 µmol of photons m^{-2} s^{-1}) and then exposed for 2 h to HL (500 µmol of photons m^{-2} s^{-1}, 2hHL) and then again shifted back to NL for 1 and 2 h (1hNL and 2hNL, respectively). Membranes isolated from the treated cells were analyzed by 1D SDS-PAGE/immunoblotting (1D blot). D1 signal was used as a loading control. Each loaded sample contained 1 µg of Chl. Antibodies specific for HliA/B, HliC, HliD, and D1 were used for immunoblotting.

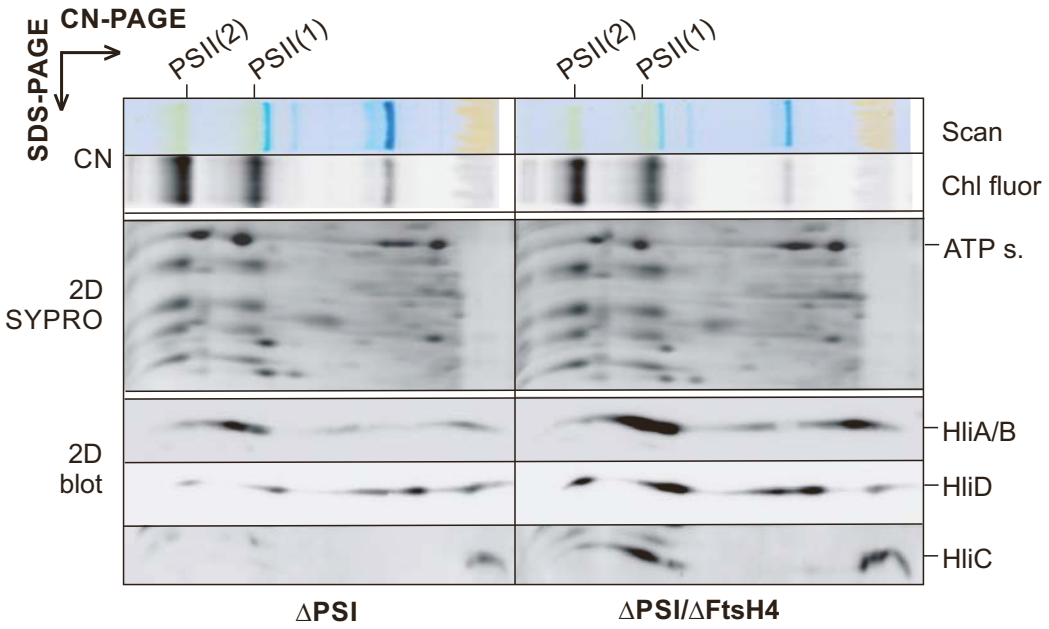

Supplementary Figure S8. Effect of *ftsH4* deletion on Hlips accumulation in PSI-less mutant. The membranes from PSI-less mutant (ΔPSI) and double mutant additionally lacking FtsH4 (ΔPSI/ΔFtsH4) grown heterotrophically at low light (5 mM glucose, 5 µmol of photons m^{-2} s^{-1}) were analyzed by 2D CN/SDS-PAGE. The CN gel was scanned (Scan) and its Chl autofluorescence detected (Chl fluor). The gel was stained by SYPRO Orange (SYPRO), electroblotted to PVDF membrane and the blot probed with antibodies specific for HliA/B, HliC, and HliD (2D blot). Each loaded sample contained 1.5 µg of Chl, the SYPRO stained gel documents the equal loading. Designation of complexes: PSII(1) and PSII(2): PSII monomer and dimer, respectively; ATP s.: α/β subunits of ATP synthase.

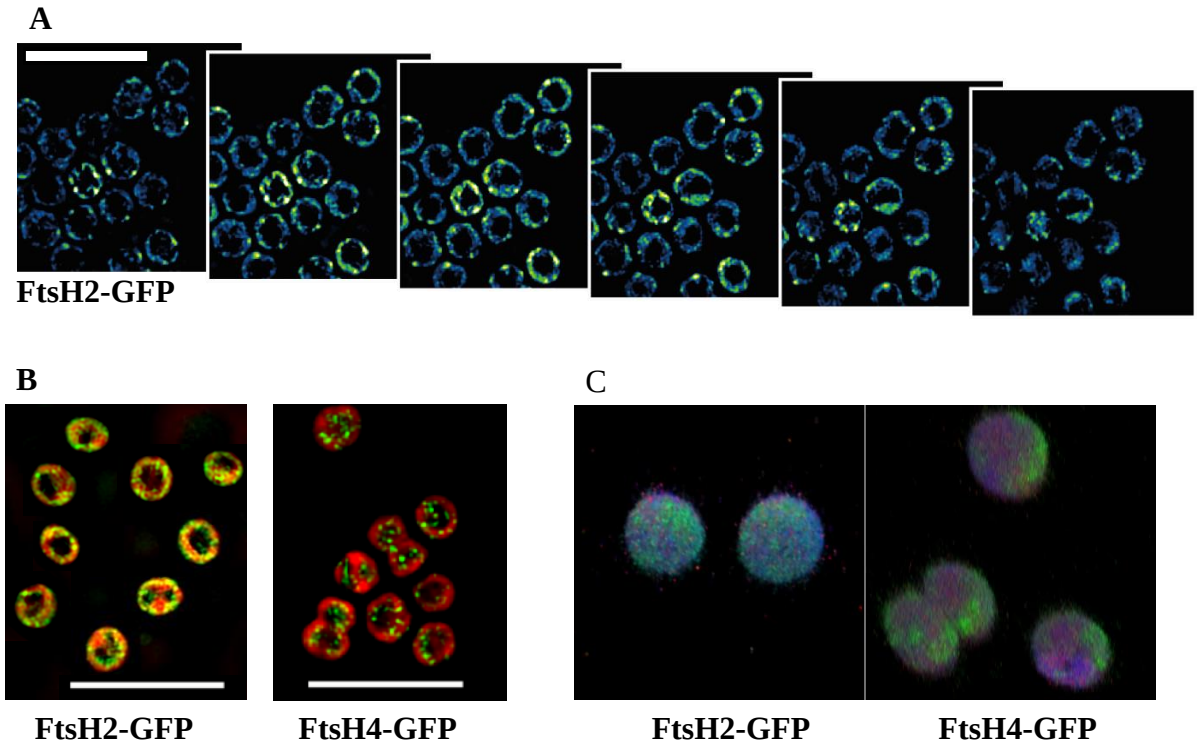

Supplementary Figure S9. Localization of FtsH2-GFP protein in *Synechocystis*. A: Axial slices used for Structured illumination microscopy (SIM) reconstructions of FtsH2-GFP (FtsH2 tagged with GFP). Descending axial slices are 125 nm apart and the scale bar is 5 µm. **B** and **C:** Comparison of FtsH2-GFP with FtsH4-GFP. **B**: 2D SIM, the overlap of the GFP signal (in green) with the chlorophyll auto-fluorescence (in red). The diffuse signal of FtsH2-GFP is present across the entire thylakoid membrane system occasionally with areas of higher intensity. Scale bar is 5 µm. **C:** 3D confocal microscopy. The overlap of the GFP signal with chlorophyll and phycobilisome auto-fluorescence in blue. Images were obtained using 8 2D slices with a thickness of 400 nm.

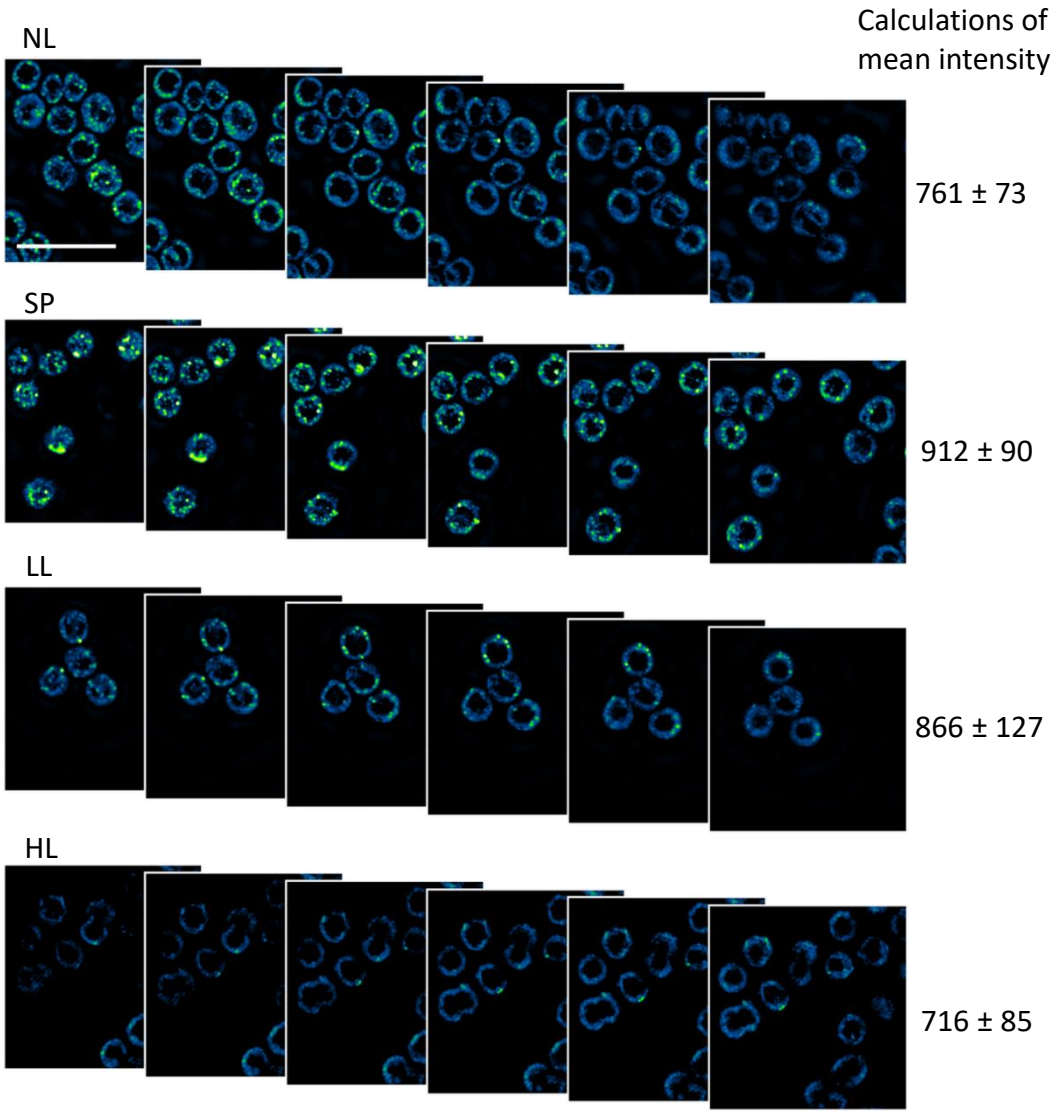

Supplementary Figure S10. Structured Illumination microscopy of FtsH4-GFP expressing cells grown under different conditions. FtsH4-GFP was imaged after acclimation to normal light (NL, 40 µmol photons m^{-2} s^{-1}), stationary phase (SP), low light (LL, 5 µmol of photons m^{-2} s^{-1}), and high light (HL, 500 µmol of photons m^{-2} s^{-1}). The images were placed on the same scale as at NL. The images are 125 nm apart axially and the scale bar represents 5 µm.

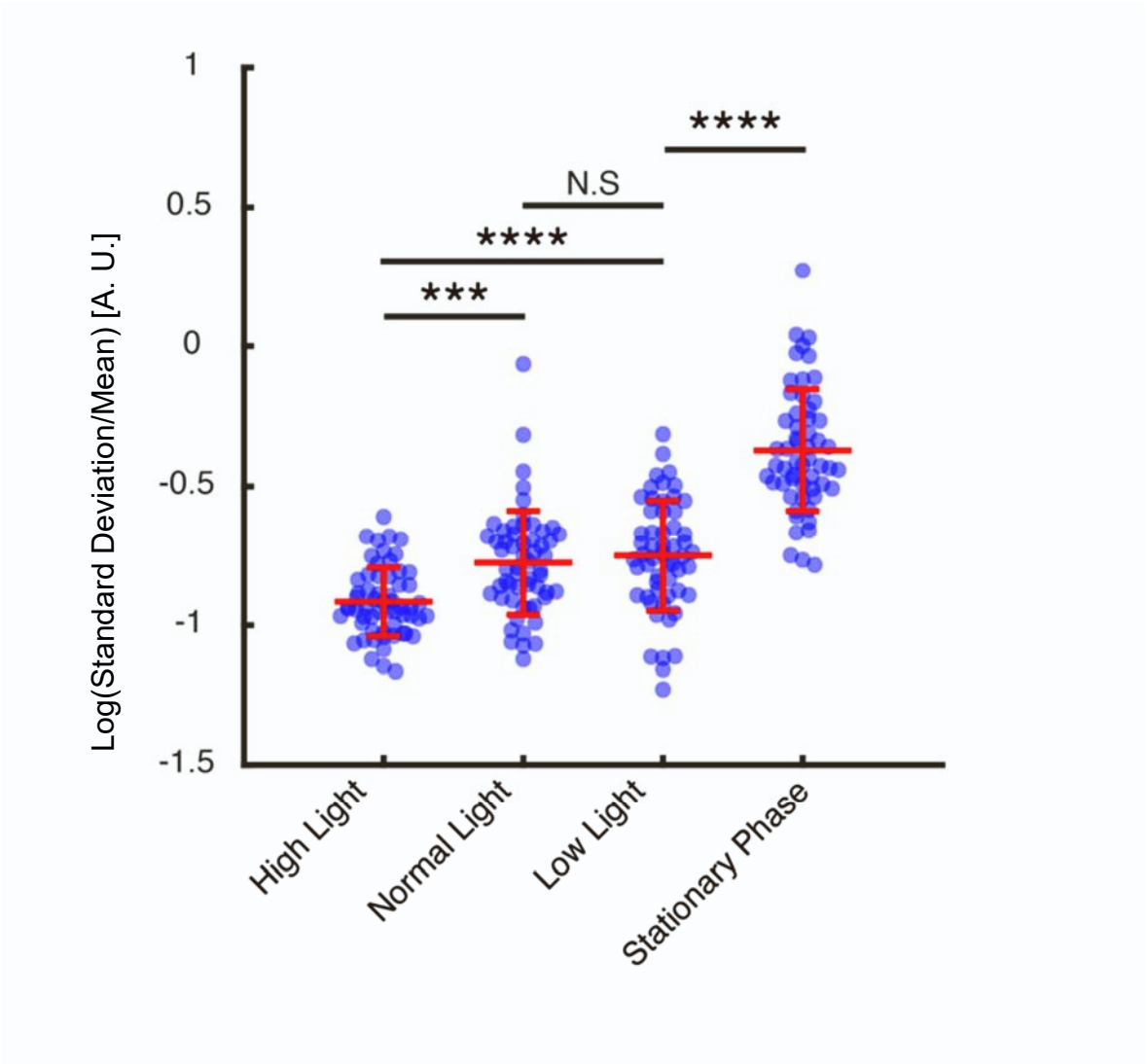

Supplementary Figure S11. Analysis of the FtsH4-GFP inhomogeneity in TM under different light conditions. The data was normalised against the mean and log-transformed. High light: 500 µmol of photons $m^{-2}s^{-1}$; Normal light: 40 µmol of photons $m^{-2}s^{-1}$; Low light: 5 µmol of photons $m^{-2}s^{-1}$. ****: P value < 5×10^{-5}; ***: $p < 5 \times 10^{-4}$; N.S.: not significant; n = 50 (50 cells represented by blue dots were analysed per each condition). P values and significance values were found with One-way ANOVA test with Tukey's Honestly Significant Difference Procedure. The error bars represent standard deviation of the calculated parameter Log(Standard Deviation/Mean).

Supplementary Tables:

Supplementary Table S1. Relative quantification of FtsH4 and core photosystem subunits in wild type *Synechocystis* thylakoid membranes.

Protein	**FtsH4**	**D1**	**D2**	**PsaA**	**PsaB**
Ratio to FtsH4	1.0	18.4	35.7	54.0	54.4
P value		0.0021	0.0034	0.0035	0.0025

Proteins extracted from thylakoid membranes were digested and the resultant proteolytic peptides analyzed by nanoLC-MS. The mass spectra were processed by searching against the *Synechocystis* sp. PCC 6803 reference proteome database using Byonic software. Relative quantification was performed by the label-free iBAQ method and expressed relative to FtsH4. P values were calculated using Student's t-test (paired, 2-sided) from 3 technical replicates (Supplementary Dataset 1).

Supplementary Table S2. Identification of major proteins in the F4CF/ΔFtsH2 FLAG pulldown resolved by SDS-PAGE.

	Protein	P value	Best score	Total Intensity	# of spectra	# of unique peptides	# of mod peptides	Coverage %	# AA's in protein
Band 1	FtsH4 (Sll1463)	1.3E-105	791	1047474290	88	31	4	61	628
Band 2	FtsH4 (Sll1463)	1.6E-93	829	1550259100	78	25	4	45	628
Band 3	FtsH4 (Sll1463)	5.1E-47	579	336645242	36	19	3	36	628

Protein bands 1, 2, and 3 (Supplementary Figure S2A) were excised and subjected to in gel digestion with trypsin. The proteolytic peptides were extracted and analyzed by nanoLC-MS and the mass spectra processed by searching against the *Synechocystis* sp. PCC 6803 reference proteome database using Byonic software. See Materials and Methods for further details. The search results are shown in the accompanying worksheets and have been filtered to remove common exogenous protein contaminants and identifications with P value > 0.05. The 'best score' refers to the highest scoring peptide spectrum match for the protein identification.

Supplementary Table S3: Relative quantification of the FtsH homologs and Sll1106 in bands obtained by separation of F4CF/ΔFtsH2 FLAG pulldown by CN-PAGE.

Protein	Percentage of FtsH4		
	Band 1	Band 2	Band 3
FtsH1/ Slr1390	0.08	0.02	0.04
FtsH3/Slr1604	0.17	0.22	0.13
FtsH4/Sll1463	100.00	100.00	100.00
Sll1106	9.77	8.23	8.98

Purified proteins were separated by CN-PAGE resulting in the three most abundant bands of approximate size 600, 820, and 900 kDa (Supplementary Fig. S2B). Band composition was analyzed by MS and the proportion of FtsH paralogs and Sll1106 was assessed by quantitative MS analysis using the sum of their iBAQ abundance scores. Relative quantification is expressed as percentage of FtsH4. For details see Supplementary Dataset 2.

Supplementary Table S4. Transcript levels of HL inducible genes in WT, ΔFtsH4, A3, and F4CF after short (30 min) and long (24 h) term HL exposure.

	WT NL	SD	ΔFtsH4 NL	SD	WT 30' HL	SD	ΔFtsH4 30' HL	SD	WT 24h HL	SD	ΔFtsH4 24h HL	SD
psbA2	0.00	0.15	0.08	0.02	1.94	0.31	1.95	0.25	0.95	0.31	0.96	0.36
psaA	0.00	0.23	0.42	0.12	-2.84	0.25	-1.25	0.53	-0.73	0.20	-0.41	0.05
ftsH2	0.00	0.08	-0.44	0.06	1.14	0.40	0.25	0.09	-2.42	0.42	-1.57	0.49
hliA	0.00	0.23	-0.33	0.04	3.86	0.69	2.36	1.36	-2.70	0.71	-1.24	0.69
hliB	0.00	0.1	-0.47	0.05	4.92	0.20	4.05	1.25	-0.18	0.49	0.92	0.52
hliC	0.00	0.09	-0.23	0.03	4.83	0.99	4.43	1.09	1.20	0.46	1.72	0.13
hliD	0.00	0.12	-0.24	0.02	1.56	0.23	1.15	0.64	-3.02	0.30	-15.27	0.56

	A3 NL	SD	F4CF NL	SD	A3 30' HL	SD	F4CF 30' HL	SD	A3 24h HL	SD	F4CF 24h HL	SD
psbA3	0.00	0.30	-0.70	0.07	1.77	0.35	2.62	0.03	2.01	0.34	1.77	0.08
psaA	0.00	0.07	-0.63	0.05	-2.18	0.01	-3.17	0.17	-0.07	0.09	-0.37	0.05
ftsH2	0.00	0.08	-0.99	0.13	0.80	0.41	2.18	1.02	-0.93	0.19	-0.51	0.04
hliA	0.00	0.30	-0.71	0.19	2.87	0.52	6.18	0.49	-0.41	0.16	-1.40	0.11
hliB	0.00	0.10	-0.02	0.20	5.71	0.42	7.23	0.66	1.18	0.07	1.43	0.09
hliC	0.00	0.15	-0.79	0.10	4.69	0.30	6.06	0.47	0.66	0.04	0.84	0.05
hliD	0.00	0.05	-0.63	0.05	-1.99	0.02	-1.21	0.03	0.21	0.10	0.07	0.02

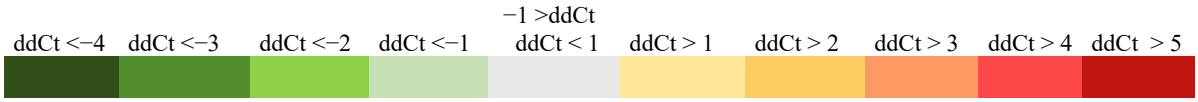

RNA was isolated from WT, ΔFtsH4, A3, and F4CF cells grown under normal light (40 µmol of photons m^{-2} s^{-1}) and after 30 min or 24 h of HL (500 µmol of photons m^{-2} s^{-1}), respectively, according to Krynická et al. (2019). Expression of *hliA/B/C/D, psbA2, psaA*, and *ftsH2* transcripts was determined by RT PCR according to Krynická et al. (2014). Random primers were used for reverse transcription. Differential expression was presented using ΔΔCt model. *rnpB* was used as an internal control. ΔΔCt represents $\Delta Ct(control) - \Delta Ct(sample)$ which corresponds to $-\log_2 FC\ (control - sample)$. WT NL was a control for all ΔFtsH4 samples and HL treated WT samples and A3 NL was a control for all F4CF samples and HL treated A3 samples. Thus, ΔΔCt of the WT NL and A3 NL matches 0. Positive/negative ΔΔCt values correspond to more/less transcript compared to control. Means of 3 independent measurements ± SD are presented.

Supplementary Table S5. iBAQ quantification of major proteins in the F4CF pulldown.

Protein	iBAQ F4CF	% of FtsH4	Factor	P Value (T-test)
FtsH4/Sll1463	155.7	100.0	1.0	
Sll1106	39.8	25.5	3.9	7.90E-04
HofG/PilA1	10.1	6.5	15.4	8.50E-04
CurT/Slr0483	5.3	3.4	29.4	3.10E-03
PsaD	3.5	2.3	43.9	7.90E-02
CP47/PsbB	2.3	1.5	66.6	8.10E-01

Proteins extracted from the FtsH4-FLAG eluate by immuno-precipitation were digested and the resultant proteolytic peptides analyzed by nanoLC-MS. The mass spectra were processed by searching against the *Synechocystis* sp. PCC 6803 reference proteome database using Byonic software. Non-specifically purified proteins (FLAG eluate from WT membranes were used as a control, Supplementary Dataset 3) were filtered from the search. Table displays the top 5 proteins specifically co-purified with FtsH4 sorted by iBAQ score (Supplementary Dataset 3). They are expressed relative to FtsH4.

Supplementary Table S6. List of primers used in this study.

construct	primer sequence
F4CF	F: CGTATCCATATGGCCATCAAACCCCAACCC
	R: TTACCATCTAGATACCACTAGGGTGCCAGGAGC
Sll1106-FLAG	F: CTAGAGCATATGAGTGACTTAATTGTTATCGGC
	R: GAGGACGCTAGCTTCCGCCGCTGGGACGCCATC
ΔFtsH4	F: ATGGCCATCAAACCCCAACCCCAATGGC
	R: TTATACCACTAGGGTGCCAGGAGCTTG
FtsH4-His	F: GACGTCGCATGCTCCCGGCCG
	R: GAGGACGGCGCCTTAATGATGATGATGATGATGTACCACTAGGGTGCCAGGAGC
FtsH4-His D515N	F: GGCCCGTTGTAAATTATTGGCCGCGCCAG
	F: CTGGCGCGGCCAATAATTTACAACGGGCC
His-HliD	F: TAATAACATATGCACCATCACCATCACCATCACCATGGAAGTGAAGAACTACAACCG
	R: GCAATAAGCCAGATCTCTAGCGCAGTCCCAACCAGG